university of groningen

University Medical Center Groningen

University of Groningen

Probing recent star formation with absorption-line strengths in hierarchical models and observations

Trager, S. C.; Somerville, R. S.

Published in:
Monthly Notices of the Royal Astronomical Society

DOI:
10.1111/j.1365-2966.2009.14571.x

IMPORTANT NOTE: You are advised to consult the publisher's version (publisher's PDF) if you wish to cite from it. Please check the document version below.

Document Version
Publisher's PDF, also known as Version of record

Publication date:
2009

Link to publication in University of Groningen/UMCG research database

Citation for published version (APA):
Trager, S. C., & Somerville, R. S. (2009). Probing recent star formation with absorption-line strengths in hierarchical models and observations. Monthly Notices of the Royal Astronomical Society, 395(2), 608-624. https://doi.org/10.1111/j.1365-2966.2009.14571.x

Copyright
Other than for strictly personal use, it is not permitted to download or to forward/distribute the text or part of it without the consent of the author(s) and/or copyright holder(s), unless the work is under an open content license (like Creative Commons).

Take-down policy
If you believe that this document breaches copyright please contact us providing details, and we will remove access to the work immediately and investigate your claim.

Downloaded from the University of Groningen/UMCG research database (Pure): http://www.rug.nl/research/portal. For technical reasons the number of authors shown on this cover page is limited to 10 maximum.

Download date: 22-05-2019

Mon. Not. R. Astron. Soc. **395,** 608–624 (2009) doi:10.1111/j.1365-2966.2009.14571.x

Probing recent star formation with absorption-line strengths in hierarchical models and observations

S. C. Trager[1⋆] and R. S. Somerville[2,3]

[1]*Kapteyn Astronomical Institute, University of Groningen, Postbus 800, NL-9700 AV Groningen, the Netherlands*
[2]*Max-Planck-Institut für Astronomie, Königstuhl 17, D-69117 Heidelberg, Germany*
[3]*Space Telescope Science Institute, 3700 San Martin Drive, Baltimore, MD 21218, USA*

Accepted 2009 January 28. Received 2009 January 19; in original form 2008 September 5

Downloaded from https://academic.oup.com/mnras/article-abstract/395/2/608/993417 by University of Groningen user on 13 December 2018

ABSTRACT

Stellar population parameters (e.g. age, metallicity and stellar abundance ratios) derived from spectral line strengths provide a powerful probe of galaxy properties and formation histories. We implement the machinery for extracting line strengths and 'single-stellar-population-equivalent' (SSP-equivalent) stellar population parameters from synthetic spectra generated by a hierarchical galaxy formation model. Our goals are (1) to test the consistency of these line-strength-derived stellar population parameters with more physically relevant light- and mass-weighted parameters for complex, cosmologically motivated star formation histories, (2) to interpret line-strength observations for early-type galaxies within the context of hierarchical structure formation and (3) to test the galaxy formation models using stellar population parameters derived from some of the best available samples of observed line strengths. We find that the SSP-equivalent age is related to the light-weighted age in a complicated fashion that reflects the influence of recently formed stars and is poorly correlated with the mass-weighted age. We find that the tendency for SSP-equivalent ages to be biased young means that 'archaeological downsizing' overstates the 'true', mass-weighted downsizing in age with mass. We find, however, that the SSP-equivalent metallicity closely tracks the mass- and light-weighted metallicities, so that observed mass–metallicity relations for old galaxies closely reflect the underlying trends. We construct mock catalogues of early-type galaxies in a Coma-cluster-sized halo and compare them directly to observations of early-type galaxies in the Coma cluster. The similarity of the SSP-equivalent ages in the observational samples and the mock catalogues gives us confidence that the star formation quenching implemented in the hierarchical galaxy formation model roughly produces the correct amount of recent star formation. Unfortunately, the current observational samples either are too small or have too low signal-to-noise ratio to accurately determine detailed star formation histories. However, the data show that the model has deficiencies: the SSP-equivalent metallicities are too low and have the wrong slope as a function of velocity dispersion, and the SSP-equivalent ages of the model galaxies may have an incorrect slope as a function of velocity dispersion. These problems are indicative both of the simplified chemical evolution prescription currently implemented in the galaxy formation model and that the star formation histories resulting from the model are incorrect in detail.

Key words: galaxies: clusters: individual: Coma – galaxies: ellipticals and lenticulars, cD – galaxies: evolution – galaxies: formation – galaxies: stellar content.

1 INTRODUCTION

The optical colours of old stellar populations are determined by an interplay between the colours of the red giant branch and the main-sequence turn-off, which together produce nearly all of the light at these wavelengths. This interplay results in the well-known age–metallicity degeneracy in old stellar populations (e.g. O'Connell 1986): a change by a factor of 2 in age looks the same in optical colours (and metal-line strengths) as a factor of 3 change in metallicity (Worthey 1994). This age–metallicity degeneracy long limited – and to some extent, still limits – our understanding

⋆E-mail: sctrager@astro.rug.nl

© 2009 The Authors. Journal compilation © 2009 RAS

of the stellar populations of 'red, dead' galaxies, like early-type galaxies.

In a pioneering paper, Rabin (1982) demonstrated that it is possible to break the age–metallicity degeneracy by using the strength of the Balmer lines of hydrogen as a function of a metal line. Ever since this breakthrough, the potential power of 'fossil' star formation evidence in local galaxies has been expected to yield insights into the formation of these objects complementary to direct look-back studies (see, e.g., the recent review by Renzini 2006). If we could measure the mass-weighted ages of local galaxies, we would know when the bulk of their stars was formed, a key constraint on galaxy formation models. This approach has yielded very interesting results when authors have applied modern stellar population models (by, e.g., Buzzoni, Mantegazza & Gariboldi 1994; Worthey 1994; Vazdekis et al. 1996; Bruzual & Charlot 2003, hereafter BC03; Thomas, Maraston & Bender 2003; Schiavon 2007 and others) to high-quality spectral observations of early-type galaxies. For example, these studies have demonstrated the wide range of galaxy ages (González 1993), the dependence of stellar population parameters (age, metallicity and abundance ratio) on galaxy velocity dispersion (Trager et al. 2000b), the dependence of age and star formation time-scale on mass (often referred to as 'fossil' or 'archaeological downsizing'; Nelan et al. 2005; Thomas et al. 2005), and the dependence of galaxy age and star formation time-scale on environment (Thomas et al. 2005; Bernardi et al. 2006; Sánchez-Blázquez et al. 2006b; but see contradictory evidence in Thomas et al. 2007).

But as age-dating techniques become more routine and confront larger data sets, the pitfalls of this approach become more apparent. The most dangerous pitfall is that the easiest and therefore most common application of these techniques assumes that galaxies can be meaningfully parametrized by a single 'age'. This assumption is in clear violation of the modern picture of galaxy formation, in which (early-type) galaxies do not form in a single burst, but are built up through a sequence of mergers (e.g. Toomre 1977; White & Rees 1978; Blumenthal et al. 1984; Kauffmann, White & Guiderdoni 1993; Cole et al. 1994; Kauffmann 1996; Kauffmann & Charlot 1998; De Lucia et al. 2006 among many others). As shown schematically by Trager et al. (2000b) and quantitatively by Serra & Trager (2007), the addition of a small fraction of young stars to an old population strongly biases the *apparent* age of a galaxy. As a simple example, the addition of 2 per cent by mass of 1-Gyr-old stars to a 12-Gyr-old population results in an apparent age of 5 Gyr (Trager, Faber & Dressler 2008, hereafter TFD08). The extreme sensitivity of stellar population ages to recent star formation (RSF) leads to ambiguities in interpretation: is a galaxy truly young or just composite, as would be expected from our current understanding of galaxy formation?[1]

Furthermore, accurate age dating, even assuming a single stellar population (SSP), requires very accurate line strengths and therefore very high signal-to-noise ratio (S/N) spectra (S/N $>$ 100 Å^{-1}; Trager 1997; Cardiel et al. 1998, 2003; Kuntschner et al. 2001). This limits its usefulness so far either to small data sets (e.g. González 1993; Kuntschner 2000; Thomas et al. 2005; Sánchez-Blázquez et al. 2006a; TFD08) or to the need to combine dozens to hundreds of galaxies together, thus losing information about dispersions in stellar population properties (e.g. Bernardi et al. 2005; Graves et al. 2007). It is therefore clear that guidance from simulations could be very useful for understanding the impact of both complex star formation histories (SFHs) and noisy data on the interpretation of stellar population ages, *if simulation results could be analysed, to the greatest extent possible, in exactly the same way as the observations*.

We turn to the latest generation of hierarchical galaxy formation models to provide this guidance. This new generation of models implements feedback from active galaxy nuclei, most importantly in the form of heating from radio jets, to solve the overcooling (e.g. Kauffmann et al. 1993) and star formation quenching (e.g. Somerville et al. 2004) problems of the previous generation of models (Bower et al. 2006; Cattaneo et al. 2006; Croton et al. 2006; Somerville et al. 2008b, hereafter S08). These models successfully predict many of the properties of local galaxies, in particular their luminosity functions, the dichotomy of galaxy colours (e.g. Strateva et al. 2001), the morphology of the colour–magnitude diagram (CMD) and even its evolution to $z = 1$. However, the authors of these papers make predictions almost solely in colour–magnitude space, which is at best a blunt tool: as discussed above, the age–metallicity degeneracy makes interpreting the colours of old populations problematic.

Now that the hierarchical galaxy formation models are doing a reasonable job at predicting basic local galaxy properties, we use these models to produce 'mock catalogues' to guide our interpretation of line-strength observations of local galaxies. We further want to subject the models themselves to a sharper test than the blunt tool of colours alone. We have two desires in this paper to make these goals concrete: (1) to use a well-defined sample of galaxies drawn from a well-understood environment that can be simply modelled in the context of the hierarchical galaxy formation models and (2) to bring the models as close to the 'observational plane' as possible. To meet the first desire, we use line-strength observations from recent samples of early-type galaxies in the Coma cluster. We choose the Coma cluster because it is a rich, well-studied cluster whose dark matter halo properties are relatively well understood (Łokas & Mamon 2003; Kubo et al. 2007). The Coma cluster is close enough to allow detailed spectroscopic study of a large number of early-type galaxies and yet is far enough that the galaxies can be treated almost as 'point sources' (but not quite; see the Appendix) in a single dark matter halo, a convenience when comparing data to hierarchical models. We will find below that the current line-strength observation samples of Coma cluster galaxies do not provide the ideal galaxy sample for our needs, but they are the best we have at the moment. To meet the second desire, we create synthetic spectra from the hierarchical galaxy formation models, based on the predicted star formation and chemical enrichment histories convolved with stellar population models, and run them through the same machinery used to extract line strengths, single-stellar-population-equivalent (SSP-equivalent) parameters and error bars on these parameters from the observed spectra. We apply this machinery to mock catalogues drawn from simulated Coma-sized haloes such that we reproduce the velocity dispersion function (VDF) of a particular observational sample. These predictions give us the sharp tool we need to understand the properties of local galaxies and to test the models themselves.

We have three goals in this paper: (1) understanding and calibrating how SSP-equivalent parameters extracted from spectral linewidths represent the underlying mass- and luminosity-weighted ages and metallicities for galaxies with complex, cosmologically

[1] Although more sophisticated methods of disentangling SFHs from spectra are becoming available (e.g. Heavens, Jimenez & Lahav 2000; Reichardt, Jimenez & Heavens 2001; Ocvirk et al. 2006; Tojeiro et al. 2007), they appear either to require very high S/N and high-resolution spectra over a long spectral baseline (Ocvirk et al. 2006; Tojeiro et al. 2007) or to produce results that are useful on average only for very large samples (e.g. Panter, Heavens & Jimenez 2003; Jimenez et al. 2007).

Downloaded from https://academic.oup.com/mnras/article-abstract/395/2/608/993417 by University of Groningen user on 13 December 2018

motivated star formation and enrichment histories, (2) interpreting line-strength observations of early-type galaxies within the context of hierarchical models and (3) using the observed line strengths for the best available samples of Coma cluster galaxies to test the physics in the galaxy formation models. This paper is organized as follows. In Section 2, we review the ingredients of the hierarchical galaxy formation models, their calibration and the stellar population modelling. In Section 3, we examine the SSP properties of composite populations from synthetic spectra created via the hierarchical galaxy formation models. In Section 4, we compare models of galaxies in the Coma cluster with observations and suggest improvements for both models and observations. Finally, in Section 5 we summarize our findings. An appendix details the aperture corrections needed to compare the resolved galaxy observations to the unresolved model galaxies.

2 HIERARCHICAL GALAXY FORMATION MODELS

We make use of a semi-analytic galaxy formation model described in detail in Somerville & Primack (1999), Somerville, Primack & Faber (2001) and S08.

2.1 Merger trees and substructure

The models are based on Monte Carlo realizations of dark matter halo merger histories, constructed using a slightly modified version of the method of Somerville & Kolatt (1999), as described in S08. The merging of subhaloes within virialized dark matter haloes is modelled by computing the time required for the subhalo to lose its angular momentum via dynamical friction and fall to the centre of the parent halo. Our treatment takes into account the mass loss of the orbiting dark matter haloes due to tidal stripping, as well as tidal destruction of satellite galaxies.

2.2 Gas cooling and star formation

When gas cools, it is assumed to initially settle into a thin exponential disc, supported by its angular momentum. Given the halo's concentration parameter, spin parameter and the fraction of baryons in the disc, we can use angular momentum conservation arguments to compute the scale radius of the exponential disc after collapse (Somerville et al. 2008a).

The models make use of fairly standard recipes for the suppression of gas infall due to a photoionizing background, cooling, star formation and supernova feedback, as described in S08. Quiescent star formation, in isolated discs, is modelled using the empirical Kennicutt star formation law (Kennicutt 1989; Kennicutt 1998):

$$\dot{\Sigma}_{\rm SFR} = A_{\rm Kenn}\, {\Sigma_{\rm gas}}^{N_K}, \quad (1)$$

with $A_{\rm Kenn} = 8.33 \times 10^{-5}$ (a factor of 2 lower than the canonical value; see S08), $N_K = 1.4$, $\Sigma_{\rm gas}$ is the surface density of cold gas in the disc (in units of $\mathrm{M_\odot\,pc^{-2}}$) and where $\Sigma_{\rm SFR}$ has units of $\mathrm{M_\odot\,yr^{-1}\,kpc^{-2}}$. We also adopt a critical surface density threshold $\Sigma_{\rm crit}$, and assume that only gas lying at surface densities above this value is available for star formation.

2.3 Galaxy mergers and morphologies

Galaxy mergers may induce a burst of star formation and destroy any pre-existing disc component, depending on the mass ratio of the smaller to the larger galaxy, μ. We parametrize the strength and time-scale of these bursts according to the results of a large suite of hydrodynamic simulations of galaxy mergers (Robertson et al. 2006; Cox et al. 2008) as described in S08. The burst efficiency is a function of the mass ratio μ and the bulge-to-total fraction of the primary galaxy (larger mass ratios yield more dramatic bursts, while the presence of a large bulge further suppresses bursts in low mass-ratio mergers); the burst time-scale is primarily a function of the primary progenitor galaxy's circular velocity (lower-circular-velocity galaxies produce longer bursts).

Mergers can also heat and thicken, or even destroy, a pre-existing disc component, driving galaxies towards morphologically earlier Hubble types. We assume that the fraction of the pre-existing stars that is transferred from a disc to a spheroidal component is a strongly increasing function of the merger mass ratio μ, such that minor mergers with $\mu < 0.2$ have little effect and major mergers with $\mu > 0.25$ leave behind a spheroid-dominated remnant.

Morphologies of the model galaxies are determined using the bulge-to-total B-band light ratios B/T following the scheme described in Kauffmann et al. (1993) and Somerville & Primack (1999), based on the results of Simien & de Vaucouleurs (1986). Galaxies with $B/T < 0.405$ are considered to be spirals, galaxies with $0.405 < B/T < 0.603$ are considered to be S0s and galaxies with $B/T > 0.603$ are considered to be ellipticals. In this paper, we consider galaxies with type S0 or E to be early-type galaxies. Note that we conservatively use B magnitudes *uncorrected* for dust extinction in this calculation. This choice moves galaxies to somewhat later morphological types (smaller B/T) as the discs are extinguished more than the bulges, so the unextinguished discs are brighter than they would be observed.

It is important to note here that although the semi-analytic model provides predictions of size estimates for disc galaxies (see S08), the model currently does not provide size estimates for bulges. Therefore, when comparing properties of local bulge-dominated (early-type) galaxies to model predictions, we must be aware of the possible effects of spatial gradients on these results. We discuss this in more detail in Section 4 and in the Appendix.

2.4 Black hole growth, supernovae and feedback

In our model, mergers also trigger the accretion of gas on to supermassive black holes (BHs) in galactic nuclei. Each top-level halo in our merger trees is seeded with a BH of mass $M_{\rm seed} \simeq 100\,\mathrm{M_\odot}$. Following a merger, the BH is allowed to grow until the radiative energy being emitted by the active galactic nuclei (AGN) becomes sufficient to halt further accretion. This self-regulated treatment of BH growth is based on hydrodynamic simulations including BH growth and feedback (Di Matteo, Springel & Hernquist 2005; Springel, Di Matteo & Hernquist 2005; Hopkins et al. 2007) and is described in more detail in S08. Because the potential well depth of the spheroid determines how large the BH has to grow in order to halt further accretion, this model successfully reproduces the BH mass versus spheroid mass relation at $z \sim 0$. Energy radiated by BHs during this 'bright', quasar-like mode can also drive galactic-scale winds, clearing cold gas from the post-merger remnants (see S08).

In addition to the rapid growth of the BH in the merger-fuelled, radiatively-efficient 'bright mode', we assume that the BH also experiences a low-Eddington-ratio, radiatively-inefficient mode of growth associated with efficient production of radio jets that can heat gas in a quasi-hydrostatic hot halo. The accretion rate in this phase is modelled assuming Bondi accretion using the isothermal cooling flow solution of Nulsen & Fabian (2000). We then assume

Downloaded from https://academic.oup.com/mnras/article-abstract/395/2/608/993417 by University of Groningen user on 13 December 2018

that the energy that effectively couples to and heats the hot gas is given by $L_{\rm heat} = \kappa_{\rm heat}\eta\dot{m}_{\rm radio}c^2$, where $\dot{m}_{\rm radio}$ is the accretion rate on to the BH, $\eta = 0.1$ is the assumed conversion efficiency of rest mass into energy and $\kappa_{\rm heat}$ is a free parameter of the order of unity.

Cold gas may be reheated and ejected from the galaxy, and possibly from the halo, by supernova feedback. The rate of reheating of cold gas is given by

$$\dot{m}_{\rm rh} = \epsilon_0^{\rm SN}\left(\frac{200\,{\rm km\,s^{-1}}}{V_{\rm c}}\right)^{\alpha_{\rm rh}}\dot{m}_*, \quad (2)$$

where $\alpha_{\rm rh} = 2$ is assumed for energy-driven winds (S08).[2] The heated gas is either trapped within the potential well of the dark matter halo and deposited in the 'hot gas' reservoir or is ejected from the halo into the 'diffuse' intergalactic medium. The fraction of reheated gas that is ejected from the halo is given by

$$f_{\rm eject}(V_{\rm vir}) = \left[1.0 + (V_{\rm vir}/V_{\rm eject})^{\alpha_{\rm eject}}\right]^{-1}, \quad (3)$$

where $\alpha_{\rm eject} = 6$ and $V_{\rm eject}$ is a free parameter in the range $\simeq$100–150 km s^{-1}. This ejected gas is reincorporated into the halo on a time-scale proportional to the halo dynamical time-scale (see S08).

2.5 Chemical evolution

Each generation of stars produces new heavy elements. The mass of metals produced is $dM_Z = y\,dm_*$, where dm_* is the mass of stars produced and y is the yield. New metals are added directly to the cold gas. When the cold gas is reheated or ejected by supernova feedback, the metals are transferred to the hot or ejected component, respectively, in the same manner as the gas. Ejected metals are also 're-accreted' by the haloes as described in S08. Note that the simple chemical enrichment model used here includes only enrichment by Type II supernovae (SNe). Therefore, the metallicities quoted should be interpreted as representing α-type elements. In this study, we assume that [E/Fe] = 0, i.e. the galaxies have solar abundance ratios and that the metallicities quoted are total metallicities. This assumption has some impact on the results discussed below, in particular on the inferred metallicities of the model galaxies. In a forthcoming paper (Arrigoni et al., in preparation), we relax this assumption and include a full galactic chemical evolution (GCE) model, tracing up to 19 individual elements. We point out below where this full GCE model differs from the present models.

2.6 Calibration

The models contain a number of free parameters, which are summarized in table 1 of S08. We adopt the '*Wilkinson Microwave Anisotropy Probe* 3' (Spergel et al. 2007) values of the cosmological parameters (S08). We then set the free parameters by matching certain observations of nearby galaxies, as described in detail in S08. For example, the star formation parameters, $A_{\rm Kenn}$ and $\Sigma_{\rm crit}$, are constrained by the observed gas fractions of nearby spiral galaxies. The supernova feedback parameters are set in order to reproduce the stellar mass fractions in low-mass haloes ($\lesssim 10^{12}\,{\rm M}_\odot$) such that the low-mass or low-luminosity slope of the observed stellar mass or luminosity function is reproduced. The yield y is set such that spiral galaxies in Milky Way sized haloes ($2 \times 10^{12}\,{\rm M}_\odot$) have approximately solar metallicity. The parameter controlling radio mode AGN feedback is set to give the minimum amount of feedback required to solve the overcooling problem and bring the high-mass or high-luminosity end of the galaxy stellar mass or luminosity function into agreement with observations. The resulting models, which are tuned solely using $z \sim 0$ observations, are also in fairly good agreement with direct probes of the mass assembly and SFH of the Universe from look-back studies based on deep cosmological surveys (S08).

2.7 Stellar kinematics

To compare model galaxy properties with observations, a useful observational tracer is the one-dimensional line-of-sight velocity dispersion, σ (hereafter referred to simply as the velocity dispersion). Velocity dispersion appears to be the controlling parameter of stellar population observables, including colour and luminosity (Bernardi et al. 2005), metallicity and abundance ratios (Trager et al. 2000b) and possibly even age (e.g. Nelan et al. 2005; Thomas et al. 2005).

Unfortunately we do not currently have detailed predictions of velocity dispersions available for our model galaxies. However, it is well known that in the local Universe, there is a tight correlation between stellar mass and velocity dispersion for early-type galaxies. We therefore simply use an empirical conversion,

$$\log\sigma = 2.2 - 0.1023\left[21.49 - \left(\frac{\log M_* - 1.584}{0.433}\right)\right]. \quad (4)$$

This relation is the result of fitting to the stellar mass and velocity dispersion data of Häring & Rix (2004) and is consistent with the results of Lintott, Ferreras & Lahav (2006) obtained from the Sloan Digital Sky Survey (SDSS). This parametrization of σ is a better approximation to the stellar velocity dispersion than estimates that simply assume that it is proportional to the velocity dispersion of the dark matter (sub)halo within the virial radius (e.g. Springel et al. 2001). Early-type galaxies are baryon-dominated so the stellar velocity dispersion can scale quite differently from the (sub)halo velocity dispersion.

2.8 Creating synthetic spectra

We convolve the resulting star formation histories (SFHs) of the model galaxies with the multimetallicity stellar spectral energy distribution (SED) models of BC03, based on the Padova1994 (Bertelli et al. 1994) isochrones with a Chabrier (2001) initial mass function (IMF), to produce synthetic spectra, broad-band magnitudes and colours, absorption-line strengths and mass-to-light ratios.

The predicted magnitudes, line-strength indices, mass-to-light ratios, light-weighted stellar population parameters and inferred SSP-equivalent stellar population parameters of the galaxy formation models are computed in a 'post-processing' step by combining the SFHs with the stellar population models. In detail, the SFHs provide a mass in stars formed at each point in a grid of ages (t) and metallicities ([Z/H]) for each galaxy in the model at the redshift of interest (in this paper, $z = 0.023$; see below). The magnitudes in photometric band k are computed as

$$M_k = -2.5\log\left(\sum_i\sum_j \mathcal{M}_{i,j}I^k_{i,j}\right) + {\rm ZP}_k, \quad (5)$$

where i, j are the age and metallicity bins, $\mathcal{M}_{i,j}$ is the mass formed at age i and metallicity j, $I^k{}_{i,j}$ is the intensity *per unit mass* in

[2] Note that there is a typographical error in this equation in S08. The expression given here is the correct one.

© 2009 The Authors. Journal compilation © 2009 RAS, MNRAS **395,** 608–624

Downloaded from https://academic.oup.com/mnras/article-abstract/395/2/608/993417 by University of Groningen user on 13 December 2018

band k for the stellar population model with age i and metallicity j and ZP_k is the magnitude zero-point for band k. We compute both dust-extinguished and -unextinguished magnitudes. We model the impact of dust on the magnitudes using an approach similar to that proposed by Charlot & Fall (2000) as modified by De Lucia & Blaizot (2007). We include two dust components, one due to 'cirrus' in the disc and one associated with the dense 'birth clouds' surrounding young star forming regions. The face-on optical depth of the 'cirrus' dust in the V band is given by

$$\tau_{V,0} \propto \tau_{\rm dust,0}\, Z_{\rm cold} m_{\rm cold}/(r_{\rm gas})^2, \quad (6)$$

where $\tau_{\rm dust,0}$ is a free parameter, $Z_{\rm cold}$ is the metallicity of the cold gas, $m_{\rm cold}$ is the mass of cold gas in the disc and $r_{\rm gas}$ is the radius of cold gas in the disc, which we assume to be 1.5 times the scale radius of the stars. We then use a 'slab' model to compute the inclination-dependent extinction (see Somerville & Primack 1999). Young stars ($t < 10^7$ yr) are additionally enshrouded in a screen of dust with optical depth $\tau_{{\rm BC},V} = \mu_{\rm BC}\tau_{V,0}$. We take $\mu_{\rm BC} = 3$. We assume a Galactic extinction curve (Cardelli, Clayton & Mathis 1989) for the cirrus component and a power-law extinction curve $A_\lambda \propto (\lambda/5500\,\text{Å})^n$, with $n = 0.7$, for the birth clouds (Charlot & Fall 2000).

Line-strength indices are computed similarly to the magnitudes as (here EW represents an equivalent width)

$$\mathrm{EW} = \Delta\left(1 - \frac{\sum_i \sum_j \mathcal{M}_{i,j} F_{\rm L}^{i,j}}{\sum_i \sum_j \mathcal{M}_{i,j} F_{\rm C}^{i,j}}\right), \quad (7)$$

where Δ is the width of the index in Å, $F_{\rm L}^{i,j}$ is the flux in the line centre for the stellar population model with age i and metallicity j and $F_{\rm C}^{i,j}$ is the flux in the continuum for that model, for indices measured in Å, and as

$$\mathrm{Mag} = -2.5\log\left(\frac{\sum_i \sum_j \mathcal{M}_{i,j} F_{\rm L}^{i,j}}{\sum_i \sum_j \mathcal{M}_{i,j} F_{\rm C}^{i,j}}\right) \quad (8)$$

for indices measured in magnitudes (Worthey 1994). We make no attempt to account for dust in the line-strength indices (MacArthur 2005).

2.9 Determining SSP-equivalent parameters

As discussed in the Introduction, the most common approach for interpreting observed spectral line strengths in terms of physical parameters that probe galaxy formation is to assume that the stellar population in a galaxy is a 'simple stellar population', i.e. it comprises stars of a single age and metallicity. Under this assumption, one can use stellar population models to derive the SSP-equivalent age and metallicity that fit the observed line strengths.

To break the age–metallicity degeneracy, we must use *both* a metal line and a hydrogen line. For the analysis herein, we use the metal-line indices Mg b, Fe5270 and Fe5335, which are more sensitive to metallicity than to age, and a Balmer-line index, which is more sensitive to age than metallicity (Worthey 1994; Worthey & Ottaviani 1997). Throughout we use the Hβ index, as this is nearly always combined with the previously mentioned metal-line indices to determine SSP-equivalent parameters (e.g. Trager et al. 2000a; Thomas et al. 2005). Using a variety of other age and metallicity indicators is beyond the scope of this paper.

We determine stellar population parameters directly using a non-linear least-squares fitting code based on the Levenberg–Marquardt algorithm described in TFD08, in which stellar population models are linearly interpolated in $(\log t, [Z/\mathrm{H}], [\mathrm{E/Fe}])$[3] on the fly to produce line strength indices (and magnitudes, colours and other parameters, but these are not typically used in the fitting process). For this purpose, we use the BC03 stellar population models modified as described in TFD08. If uncertainties in the stellar population parameters are desired, they are computed by taking the dispersion of stellar population parameters from 10 000 Monte Carlo trials using the provided index errors as 1σ Gaussian deviates. We compute the stellar population quantities for both the entire galaxy ('total') and its bulge component ('bulge'). Finally, we compute light-weighted stellar population parameters for each photometric band by combining the SFHs with the SEDs.

2.10 Coma cluster model

For the analysis in this paper, we are interested in comparing our models with real observations of early-type galaxies. The Coma cluster is a convenient target, as a large body of reasonable to excellent quality line-strength data is available (e.g. see the compilation in TFD08). We therefore generated 20 realizations of a Coma-cluster-sized halo, i.e. a halo with a circular velocity $V_{\rm c} = 1066\,\mathrm{km\,s^{-1}}$, corresponding to a virial mass of $M_{\rm vir} = 10^{14.9}\,\mathrm{M}_\odot$, similar to if slightly lower than recent estimates of the mass of the Coma cluster (Łokas & Mamon 2003; Kubo et al. 2007, and references therein). The smallest haloes that we resolve in our merger trees have a virial mass of $10^{10}\,\mathrm{M}_\odot$, so we select galaxies with $M_* > 10^9\,\mathrm{M}_\odot$, corresponding to a velocity dispersion $\sigma = 57\,\mathrm{km\,s^{-1}}$ using equation (4). We select only 'early-type' galaxies (E and S0) according to their B-band bulge-to-total light ratios, as described in Section 2.3. We set the output redshift of the simulations to be $z = 0.023$ (e.g. Hudson et al. 2001) to match the redshift of the Coma cluster.

3 SINGLE-STELLAR-POPULATION PROPERTIES OF GALAXIES IN HIERARCHICAL MODELS

In this section, we seek to understand the properties of composite stellar populations when interpreted using SSP-equivalent parameters. This can be thought of as extending the work of Serra & Trager (2007) to more complicated – and hopefully more realistic – SFHs. We first examine the SFHs and metallicity distributions of galaxies drawn from semi-analytic models, then examine their absorption-line strengths and inferred SSP-equivalent ages and compare these with the intrinsic physical time-scales predicted by the semi-analytic models, such as luminosity- and mass-weighted ages, merger times and birthrates.

3.1 Star formation histories and metallicity distributions

We begin by displaying the average SFHs and metallicity distributions of early-type galaxies in Coma-cluster-sized haloes in Fig. 1. In the upper panel, we find clear evidence for 'downsizing' in the peak star formation epoch of early-type galaxies drawn from the semi-analytic models: the more massive the galaxy, the earlier (on average) the peak in the SFH (compare with the top panel of

[3] Recall that the galaxy formation models have solar abundance ratios and therefore $[\mathrm{E/Fe}] = 0$, although this is not true for the galaxy observations described later.

Downloaded from https://academic.oup.com/mnras/article-abstract/395/2/608/993417 by University of Groningen user on 13 December 2018

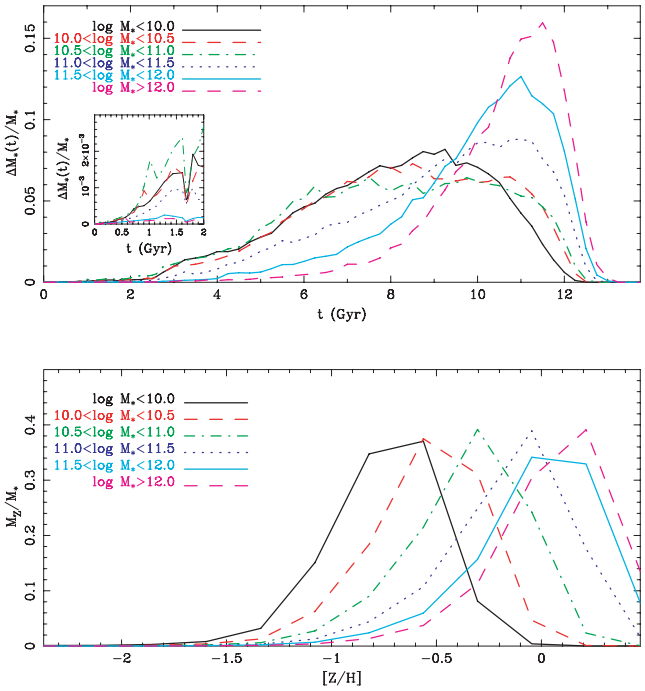

Figure 1. Average SFHs (top panel) and metallicity distributions (bottom panel) for early-type galaxies in 20 realizations of a Coma-cluster-sized halo, binned by stellar mass. The inset in the top panel shows the recent low-level star formation in lower-mass model galaxies. Time in these panels is age or equivalently look-back time. 'Downsizing' is clear in these simulated galaxies: the age of the peak of the SFH decreases with decreasing mass, although this decrease flattens out at the smallest masses. A mass–metallicity relation is also apparent in the average metallicity distributions, with a 'kink' and flattening in the peak metallicities around $M_* \sim 10^{11}\,\mathrm{M}_\odot$.

fig. 1 in De Lucia et al. 2006, who found similar results using a similar hierarchical galaxy formation model including AGN feedback, although many of the details are different). The inset in the upper panel shows the SFHs of the galaxies over the last 2 Gyr, the time-scale to which Hβ and the other Balmer lines are maximally sensitive (e.g. Serra & Trager 2007, and Fig. 7); note that the lower the mass, the more likely the galaxy is to still have some ongoing star formation at these late times. In the current models, however, downsizing is not very apparent at masses below $M_* \lesssim 10^{11}\,\mathrm{M}_\odot$, and galaxies with masses $M_* \sim 10^{11}\,\mathrm{M}_\odot$ have the highest fraction of recent ($t < 2$ Gyr) star formation. In the lower panel, we see clear evidence for a mass–metallicity relation in the early-type galaxies: low-mass galaxies have lower metallicities than high-mass galaxies, as expected (Faber 1973). Furthermore, it is clear that there is a 'kink' in the relation at a mass of $M_* \sim 10^{11}\,\mathrm{M}_\odot$ and a flattening above this mass (note the spacing of the peak of the metallicity distributions; also compare Fig. 8 with fig. 8 in Gallazzi et al. 2005).

3.2 Line strengths and SSP analysis

Using the procedure detailed in Section 2.8 above, we have computed line-strength indices for simulated early-type galaxies in Coma-cluster-sized haloes. The results for Hβ, Mg b and ⟨Fe⟩ are shown in Fig. 2. The left-hand panel shows that there is a weak trend in metallicity as a function of age, although with a large scatter. This is in the sense that lower-metallicity galaxies have younger ages, and originates mainly from the trends between galaxy mass and metallicity and galaxy mass and age in the models (low-mass galaxies are both younger and more metal-poor). The right-hand panel of Fig. 2 shows only that the enhancement ratios of the model galaxies are solar, i.e. [E/Fe] = 0. This is not surprising, since we have used solar abundance SSP models to generate the synthetic spectra.

Fig. 3 shows the three derived stellar population parameters (age, metallicity and [E/Fe]) plotted against the galaxy velocity dispersion. The SSP-equivalent ages of the model galaxies decrease with decreasing velocity dispersion, a phenomenon often referred to as 'archaeological downsizing' (cf. Nelan et al. 2005; Thomas et al. 2005, among others). The scatter also grows with decreasing velocity dispersion, suggesting that the formation of low-mass galaxies is typically more extended than that of higher-mass galaxies (as we saw in Fig. 1). The SSP-equivalent metallicities show a tight and strong mass–metallicity relation, as expected (see above), but the slope is steeper and the zero-point is lower than the real Coma cluster data shown by the dashed lines (we discuss this point further below and in Section 4.4).

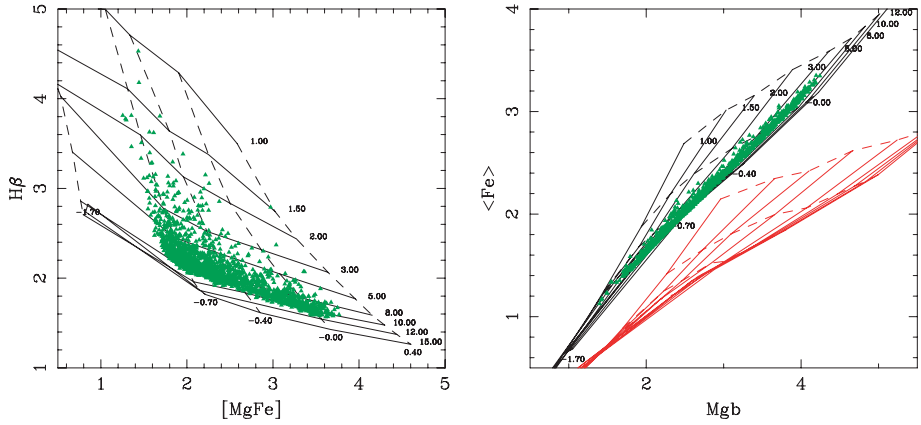

Figure 2. Line-strength indices of simulated early-type galaxies from 20 realizations of a Coma-cluster-sized halo. Left-hand panel: the Hβ–[MgFe] diagram is a convenient plot from which to read SSP-equivalent age (solid, roughly horizontal lines) and SSP-equivalent metallicity (dashed, roughly vertical lines), as these indices are at best only mildly affected by [E/Fe] ≠ 0 (Trager et al. 2000a; Thomas, Maraston & Korn 2004). Right-hand panel: the Mg b–⟨Fe⟩ diagram is a convenient plot from which to read [E/Fe]. The left-hand grid in this panel has [E/Fe] = 0 (i.e. solar composition) and the right-hand grid has [E/Fe] = +0.3. Note that these model galaxies show no evidence for [E/Fe] ≠ 0, as expected from the chemical evolution prescription used in the simulation (see text).

© 2009 The Authors. Journal compilation © 2009 RAS, MNRAS **395,** 608–624

Downloaded from https://academic.oup.com/mnras/article-abstract/395/2/608/993417 by University of Groningen user on 13 December 2018

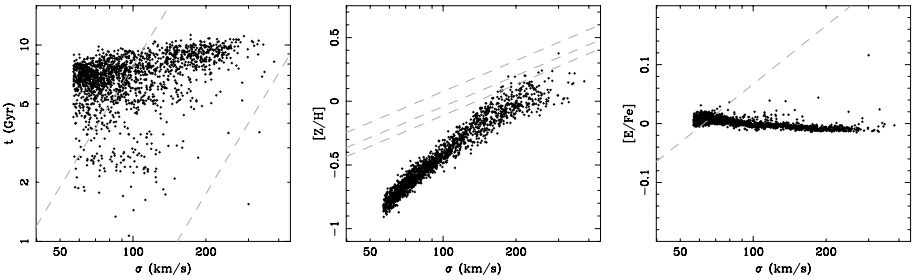

Figure 3. Velocity-dispersion–stellar-population-parameter relations for model early-type galaxies selected from an ensemble of 20 realizations of a Coma-cluster-sized halo. The dashed lines are projections of the observed Coma cluster Z plane (for metallicities of $[Z/H] = -0.5, 0, +0.5$ dex in the left-hand panel and ages of 5, 10, 15 Gyr in the middle panel) and $[E/Fe] - \sigma$ relation (right-hand panel) on to the relations (see Trager et al. 2000b; TFD08). One can see 'archaeological downsizing' in the left panel, along with a steeper mass–metallicity relation than seen in the data (middle panel). Note that the point with high [E/Fe] in the right-hand panel is also the object with very young age and high velocity dispersion ($\sigma \approx 300\,\mathrm{km\,s^{-1}}$) in the left-hand panel: it falls in a slightly unusual region of line-strength space because of a burst of RSF and has a biased [E/Fe] as a result, even though intrinsically it has $[E/Fe] = 0$.

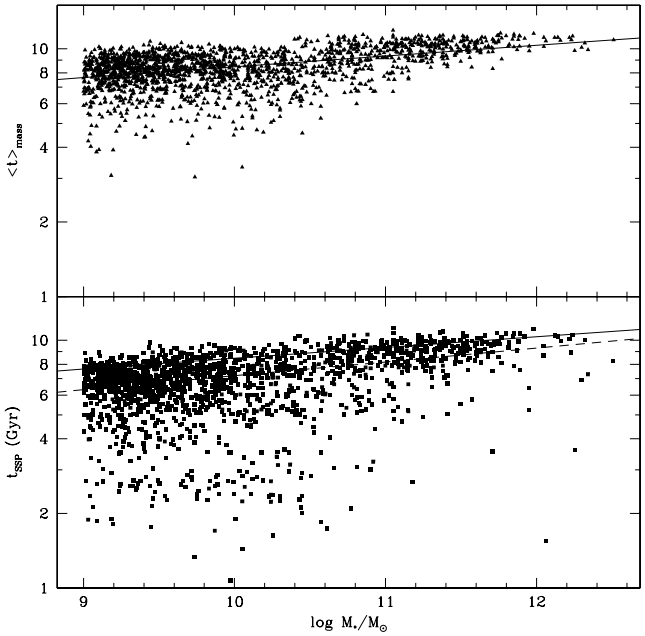

Figure 4. Mass–age relations for model early-type galaxies drawn from 20 realizations of a Coma-cluster-sized halo. Top panel: mass-weighted stellar age as a function of stellar mass. The solid line is a 3σ-clipped least-squares fit. The relation is quite shallow and possibly even flat below $M_* = 10^{10}\,\mathrm{M}_\odot$. Bottom panel: SSP-equivalent stellar population age as a function of stellar mass. The dashed line is a 3σ-clipped fit to these points, and the solid line is the fit from panel (a). Note the large scatter in t_{SSP}, the lower apparent ages and the strong apparent 'archaeological downsizing', which exaggerates the trend actually present in the mass-weighted ages.

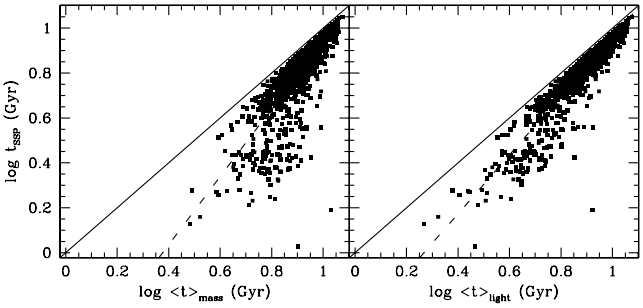

Figure 5. SSP-equivalent age as a function of mass-weighted (left-hand panel) and (V-band) light-weighted (right-hand panel) age for model early-type galaxies drawn from 20 realizations of a Coma-cluster-sized halo. Solid lines are lines of equivalence for the plotted parameters and dashed lines are linear-least-squares fits given in equations (9) (left-hand panel) and (10) (right-hand panel). The SSP-equivalent and light-weighted ages are correlated, as are the SSP-equivalent and mass-weighted ages, but the scatter is very large, the slope is not unity and the SSP-ages are biased low. The scatter is larger for the more physically interesting mass-weighted ages. These biases are due to residual star formation in some fraction of the early-type galaxies (cf. Serra & Trager 2007).

3.2.1 'Archaeological downsizing' and recent star formation

Given the known sensitivity of Balmer lines to recent star formation (RSF; e.g. Trager et al. 2000b; Serra & Trager 2007), we ask whether the 'archaeological downsizing' seen in these models is a reflection of true downsizing in the mass-weighted ages of the (model) galaxies or just results from small amounts of star formation occurring preferentially in smaller galaxies with extended SFHs. In Fig. 4, we see that the latter case is likely to be the dominant signal in 'archaeological downsizing' in these models: low-mass galaxies have more RSF than high-mass galaxies, as expected from Fig. 1, resulting in younger SSP-equivalent ages. This can be seen even more clearly in the left-hand panel of Fig. 5, which shows that the SSP-equivalent ages of galaxies are *always* younger than the mass-weighted ages, with the discrepancy (and scatter) growing towards younger – and thus lower-mass, following Fig. 4 – galaxies. We suggest therefore that 'archaeological downsizing' will always appear stronger than any true (mass-weighted) downsizing in the stellar populations due to the bias caused by RSF in low-mass galaxies. This is not to say that downsizing does not happen in these models – it clearly does, as shown in the top panel of Fig. 4 – rather that 'archaeological downsizing' results (such as Nelan et al. 2005; Thomas et al. 2005) almost certainly overstate the true magnitude of downsizing, as suggested by TFD08.

Further examining Fig. 5, we find that the SSP-equivalent ages of model galaxies are in fact correlated with both the mass- and light-weighted ages of the galaxies, but the scatter is large in both cases (especially for the mass-weighted ages), as expected from the preceding discussion. Simple linear fits to the points in Fig. 5 give the following relations:

$$\log t_{\mathrm{SSP}} = 1.51\,(\pm 0.02)\,\log\langle t\rangle_{\mathrm{mass}} - 0.568\,(\pm 0.002) \qquad (9)$$

$$\log t_{\mathrm{SSP}} = 1.31\,(\pm 0.01)\,\log\langle t\rangle_{\mathrm{light}} - 0.351\,(\pm 0.001) \qquad (10)$$

for 1801 model galaxies, where the uncertainties are formal 1σ errors assuming equal weighting of points in the least-squares fits

Downloaded from https://academic.oup.com/mnras/article-abstract/395/2/608/993417 by University of Groningen user on 13 December 2018

and the rms scatters are 0.08 and 0.05 dex, respectively. We note the following points.

(i) As discussed above, RSF strongly biases the inferred ages, such that SSP-equivalent ages are younger than mass-weighted ages by more than 40 per cent on average and younger than light-weighted ages by roughly 25 per cent on average, thus greatly exaggerating the effect of downsizing on the stellar population ages.

(ii) The scatter is asymmetric in both diagrams. As discussed by Serra & Trager (2007), galaxies that appear young in $t_{\rm SSP}$ are not guaranteed to be – and in these simulations, unlikely to be – young in a mass- or light-weighted sense.

(iii) The biases can be expected to be even worse for smaller samples of galaxies. As an example, we consider the relations between SSP-equivalent and mass- or light-weighted age for a mock catalogue representing the Moore et al. (2002) sample of Coma cluster galaxies (see Section 4.3). For this sample of 108 (model) galaxies, the slopes of the relations are steeper [$\log t_{\rm SSP} \propto (1.89 \pm 0.25) \log \langle t \rangle_{\rm mass}$ and $\log t_{\rm SSP} \propto (1.53 \pm 0.15) \log \langle t \rangle_{\rm light}$] and the scatters are larger (0.18 and 0.16 dex, respectively).

If the SSP-equivalent age of a galaxy does not accurately represent its mass- or light-weighted age, is there some other relevant time-scale of its SFH that it does reflect? Using our knowledge of the mass and SFHs of the model galaxies, in Fig. 6 we present $t_{\rm SSP}$ as a function of the times of the last merger (mass ratio greater than 1:10) and the last major merger (mass ratio greater than 1:5), and the times at which 50 and 80 per cent of the present-day stars were formed. The correlations of $t_{\rm SSP}$ with these quantities are even worse than with the mass- or light-weighted ages. In the case of the merger times, recent dry mergers leave $t_{\rm SSP}$ relatively unchanged, while minor but gas-rich mergers can seriously perturb $t_{\rm SSP}$. The lack of a strong correlation of $t_{\rm SSP}$ with the times at which 50 and 80 per cent of the present-day stars are formed is again due to the presence of RSF. If the last small fraction of stellar mass is formed recently in a galaxy, this RSF results in a young $t_{\rm SSP}$.

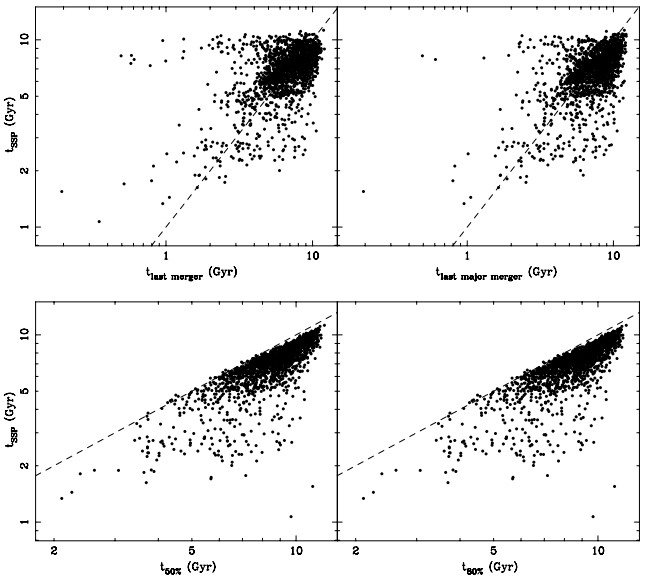

Figure 6. Comparison of SSP-equivalent age with galaxy assembly time-scales. Top panels: $t_{\rm SSP}$ as a function of the time of last merger (left-hand panel) and the time of last major merger (right-hand panel). Bottom panels: $t_{\rm SSP}$ as a function of the time at which 50 per cent of stellar mass was formed (left-hand panel) and the time at which 80 per cent of stellar mass was formed (right-hand panel).

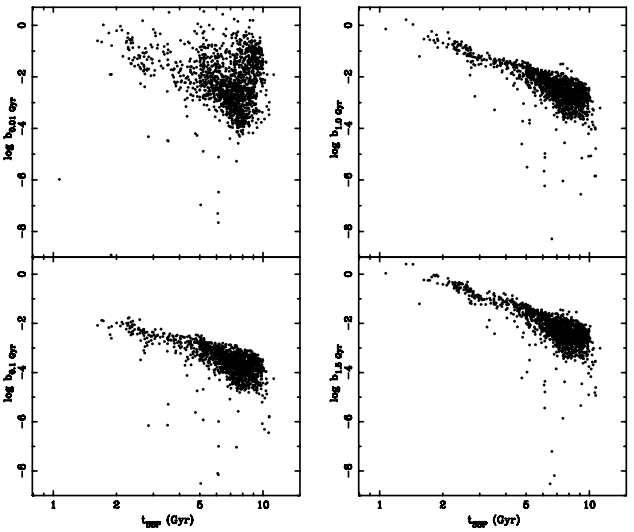

Figure 7. Correlation of SSP-equivalent age and 'birthrate' parameter, which is the star formation rate (SFR) averaged over a relatively short time-scale τ, divided by the SFR over the whole lifetime of the galaxy. Top-left panel: birthrate with $\tau = 10$ Myr ($b_{0.01\,\rm Gyr}$). Bottom-left panel: birthrate with $\tau = 100$ Myr ($b_{0.1\,\rm Gyr}$). Top-right panel: birthrate with $\tau = 1.0$ Gyr ($b_{1.0\,\rm Gyr}$). Bottom-right panel: birthrate with $\tau = 1.0$ Gyr ($b_{1.5\,\rm Gyr}$). (Galaxies with no star formation within the appropriate time-scale are not plotted.) The correlation of $t_{\rm SSP}$ with $b_{0.1\,\rm Gyr}$, $b_{1.0\,\rm Gyr}$ and $b_{1.5\,\rm Gyr}$ highlights the sensitivity of the SSP-equivalent age to RSF.

Rather than a specific event in the history of the galaxy, the SSP-equivalent age represents a rough measure of the birthrate of stars over the last 1–1.5 Gyr. This can be seen in Fig. 7, where we plot the average birthrate $b_{\rm t}$ – the fraction of stellar mass formed over some time with respect to the total stellar mass – for four time-scales: 0.01, 0.1, 1.0 and 1.5 Gyr. We see that the best correlation of $t_{\rm SSP}$ with $b_{\rm t}$ is when $1 < t < 1.5$ Gyr, suggesting that SSP-equivalent ages inferred from Hβ are maximally sensitive to RSF in the past Gyr (as shown from simpler, two-burst models in Serra & Trager 2007). We therefore conclude that $t_{\rm SSP}$ is mostly measuring RSF over $\sim$1 Gyr time-scales, not mass- or light-weighted ages, not merger times and not the time at which some (large) fixed fraction of stellar mass has formed.

3.2.2 Metallicities

We turn briefly to the metallicities of the model galaxies. We present their mass–metallicity relations in Fig. 8 for both the mass-weighted and SSP-equivalent metallicities. As expected from the bottom panel of Fig. 1, a distinct flattening of the relations occurs at masses above $\log(M_*/{\rm M}_\odot) \gtrsim 11.3$. This is in rough accordance with the results of Gallazzi et al. (2005), who found a similar effect in the r-band-luminosity-weighted metallicities of SDSS galaxies (see also fig. 6 of S08). Our (V-band) light-weighted metallicities are slightly too low as compared with the data; the difference in the scatter is due to observational uncertainties in the SDSS data that we have not attempted to model. However, our intent here is not to make a detailed comparison with the SDSS data; rather, we will generate mock catalogues to compare with the Coma cluster galaxies in Section 4.4.

We compare mass- and light-weighted metallicities with SSP-equivalent metallicities in Fig. 9. Unlike in the case of $t_{\rm SSP}$, $[Z/{\rm H}]_{\rm SSP}$ correlates almost perfectly with mass- and light-weighted metallicity (as shown in Serra & Trager 2007), with very small scatter in the

Downloaded from https://academic.oup.com/mnras/article-abstract/395/2/608/993417 by University of Groningen user on 13 December 2018

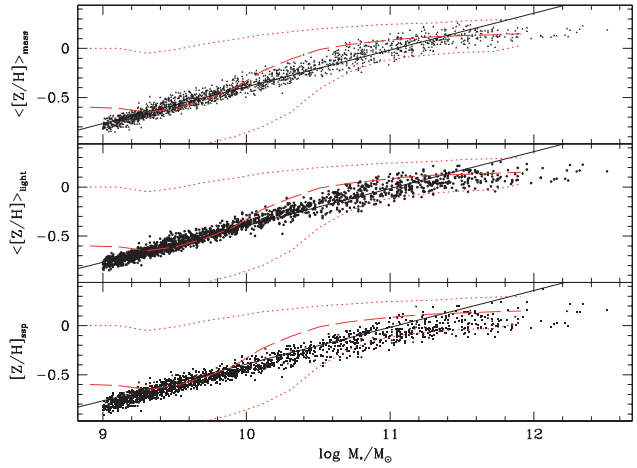

Figure 8. Mass–metallicity relations for model early-type galaxies drawn from 20 realizations of a Coma-cluster-sized halo. Top panel: mass-weighted metallicity as a function of stellar mass. The solid line is a 3σ-clipped least-squares fit to the relation. There is clearly a very strong, tight mass–metallicity relation which flattens out at masses above $M_* \sim 3 \times 10^{11}\,\mathrm{M}_\odot$. The long-dashed (red) line is the mass-r-band-light-weighted–metallicity relation from the SDSS sample of Gallazzi et al. (2005) and the dotted (red) lines are the 1σ marginalized confidence bounds on this relation. Middle panel: V-band light-weighted metallicity as a function of stellar mass. Solid, long-dashed and dotted lines are the same as in the top panel. Note that the model light-weighted metallicities are slightly too low as compared with the SDSS galaxies. Bottom panel: SSP-equivalent stellar population metallicity as a function of stellar mass. Solid, long-dashed and dotted lines are again the same as in the top panel. The scatter is slightly larger, the slope is slightly flatter and the zero-point is slightly lower than for the mass–mass-weighted-metallicity relation.

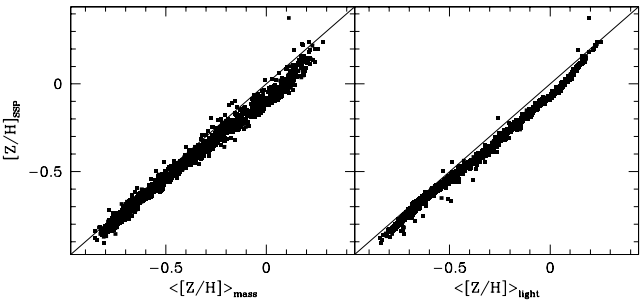

Figure 9. SSP-equivalent metallicity as a function of mass-weighted (left-hand panel) and (V-band) light-weighted (right-hand panel) metallicity for model early-type galaxies drawn from 20 realizations of a Coma-cluster-sized halo. Solid lines are lines of equivalence for the plotted parameters. The SSP-equivalent metallicities correlate well with mass- and light-weighted metallicities, albeit with a small offset.

latter case. The SSP-equivalent metallicity is therefore a very good tracer of the light- or even mass-metallicity of a galaxy, modulo a small offset towards lower metallicity.

Finally, we turn to the Z plane of Trager et al. (2000b), a relation between velocity dispersion and SSP-equivalent age and metallicity. In Fig. 10, we present these quantities projected on to the Z plane of Coma cluster early-type galaxies determined in TFD08. The left-hand panel shows that the metallicities of the model galaxies are too low at a given velocity dispersion, while the right-hand panel shows that the slope of the edge-on view of the Z plane of the model galaxies is too shallow as compared with the observations. The former problem is due to the chemical evolution model used

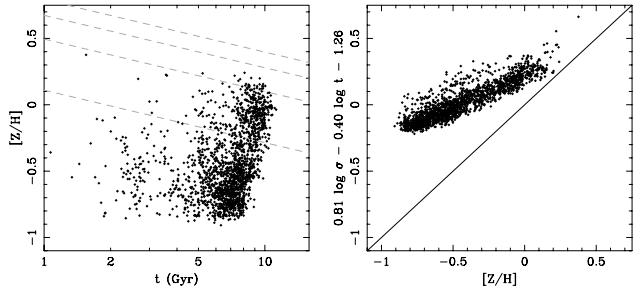

Figure 10. A nearly face-on (left-hand panel) and the edge-on (right-hand panel) view of the Z plane (Trager et al. 2000b) for model galaxies from the ensemble of 20 realizations of a Coma-cluster-sized halo. The dashed lines in the left-hand panel are projections of the observed Coma cluster Z plane (TFD08) on to the age–metallicity plane for $\sigma = 50, 150, 250, 350\,\mathrm{km\,s^{-1}}$. The solid line in the right-hand panel is the edge-on view of the Z plane. At a given velocity dispersion, model metallicities are typically too low with too steep of a slope, as seen in the middle panel of Fig. 3.

and assumptions about the IMF. Arrigoni et al. (in preparation) have shown that a more detailed, multi-element chemical evolution model that includes enrichment by Type Ia SNe and a slight flattening of the IMF (to produce more high-mass stars and therefore more metals) can remove this discrepancy. The latter problem is either due to the wrong mass–metallicity slope (which seems unlikely from Fig. 8) or due to a different correlation between t_{SSP} and $[Z/\mathrm{H}]_{\mathrm{SSP}}$ in the data and models. We consider these possibilities in more detail below.

4 COMA CLUSTER: OBSERVATIONS AND MOCK CATALOGUES

We now turn to our second and third goals, which are interpreting the properties of local early-type cluster galaxies in the context of hierarchical formation models and testing the models themselves using the data.

4.1 Colour–magnitude diagram

To begin our confrontation between the models and data, we ask whether the current galaxy formation models can reproduce the CMD of galaxies – regardless of morphology or colour – in the Coma cluster. In Fig. 11, we show the magnitudes and colours of galaxies drawn from a single Coma-sized halo overlaid on the CMD of Coma cluster galaxies drawn from the sixth data release (DR6) of the SDSS (Adelman-McCarthy et al. 2008). We divide the CMD into red and blue regions using the magnitude-dependent cut of Baldry et al. (2004), which provides a fairly clean separation of both the model and Coma cluster galaxies. We see that the slope of the red sequence of model galaxies matches the Coma cluster galaxies very well. The model galaxies appear to be slightly too blue, which is likely due to the too low metallicities of galaxies in the model. There are also not enough truly blue galaxies down to the limits of the model and the spectral data. However, this may be due to the fact that the model galaxies are selected down to a fixed stellar mass, not a given luminosity. As blue galaxies have low mass-to-light ratios, star-forming galaxies with masses below our mass limit can have luminosities higher than red galaxies above our mass limit. The good (if not perfect) match between the model and observed CMDs gives us confidence to proceed with attempting to match detailed stellar population properties. We note that the luminosity

Downloaded from https://academic.oup.com/mnras/article-abstract/395/2/608/993417 by University of Groningen user on 13 December 2018

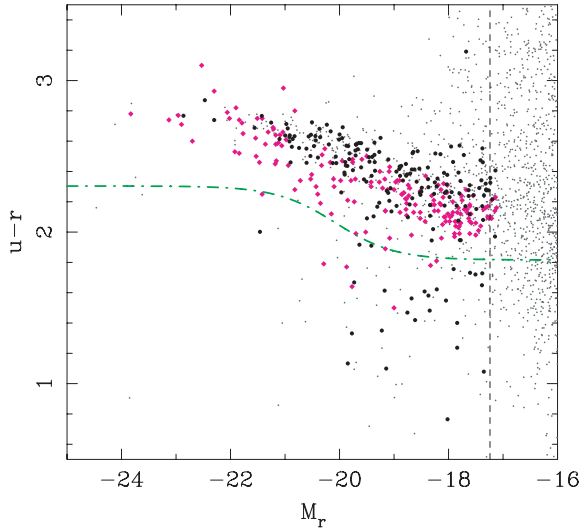

Figure 11. Observed and predicted CMD of the Coma cluster. Large black dots show galaxies with redshifts from the SDSS DR6 (Adelman-McCarthy et al. 2008), placing them at the distance of the Coma cluster; small grey points are other galaxies in the same field without DR6 redshifts, assuming that they are also in the cluster; and (pink) diamonds are model galaxies drawn from a single realization of a Coma-cluster-sized halo, with no regard to morphology or colour. The dot–dashed green line demarcates the blue-red galaxy division of Baldry et al. (2004); note the excellent agreement of the model and observed red sequence slope and good agreement of the zero-points. The dashed vertical line represents the magnitude limit of SDSS spectroscopy, which is close to the model-galaxy mass selection limit of $10^9\,\mathrm{M}_\odot$.

function predicted by the model is also in good agreement with the observed Coma luminosity function.

4.2 Observational material

To compare the hierarchical galaxy formation models with observed stellar population parameters of early-type Coma cluster galaxies, we use the data presented in TFD08, concentrating on three samples: the Low-Resolution Imaging Spectrometer data of TFD08 ('the LRIS sample'), which have excellent quality (in terms of S/N) but only 12 galaxies; the large, morphologically selected, complete sample of Moore et al. (2002, 'the Moore sample'), of somewhat poorer quality than the LRIS sample but containing 10 times as many galaxies; and the large, red-sequence-selected sample of Nelan et al. (2005, 'the Nelan sample'), again of poorer quality than the LRIS sample but again much larger. Characteristics of these three samples are presented in Table 1.

The line strengths of the LRIS sample galaxies have been adjusted to represent those taken through an aperture with radius equal to one-fourth of the effective radius ($r = r_\mathrm{e}/4$) of each galaxy (see TFD08 for more details on the method, and note that the apertures in that paper are denoted in diameters, not radii). This has been done in an attempt to fairly compare the 'global' stellar populations of the Coma cluster galaxies with the simulated galaxies, which are unresolved and therefore should be considered to represent 'global' properties. The $r_\mathrm{e}/4$ aperture does not perfectly represent the 'global' properties, but we show in the Appendix that stellar populations observed through apertures with radii $r = r_\mathrm{e}$ are typically negligibly older and 0.10 dex more metal-poor. The line strengths of the Moore and Nelan samples were taken through fibre diameters of 2.7 and 2.0 arcsec; the typical 'global' ages and metallicities (i.e. taken through an aperture of radius r_e) for these apertures are again negligibly older and 0.10 dex more metal-poor. We will refer to these shifts from observed to 'global' parameters below.

4.3 Mock catalogues

To make the desired comparison in a sensible way, we construct mock catalogues of early-type galaxies selected from the simulations. These mock catalogues consist of model galaxies selected to be early-type galaxies by the criteria discussed in Section 2.3 above or red-sequence galaxies (see below) and to have the same VDF as the observed galaxies. A VDF is merely the histogram of (logarithmic) velocity dispersions $\log\sigma$ with a specified bin width; in this paper, we use a bin size of $\Delta\log\sigma = 0.05$ dex. As much as is possible, the mock catalogue is constructed such that each bin in the VDF is sampled from the simulated galaxies with the appropriate velocity dispersions without replacement. Only when a VDF bin is less populated in the simulation than in the observations are galaxies selected from the simulation more than once (although these galaxies will have different index strengths due to the assumed index errors; see below). If there are no simulated galaxies in a VDF bin populated by the observed galaxies, as can be the case at the highest (typically cD galaxies) and lowest velocity dispersions, no galaxies are added to the mock catalogue. As noted in Section 2.7, the mass limit of our simulations is $M_* > 10^9\,\mathrm{M}_\odot$, corresponding to $\sigma > 57\,\mathrm{km\,s^{-1}}$. Galaxies with velocity dispersions lower than this limit are not included in the mock catalogues. An example of the result of our selection algorithm is given in Fig. 12 for the mock catalogue of the Moore et al. (2002) sample.

The Nelan sample is a colour- and magnitude-limited sample designed to select red-sequence galaxies (Smith et al. 2004). Galaxies in this sample were selected to have $R_\mathrm{c} < 17$ mag and colours redder than $\Delta(B - R_\mathrm{c}) > -0.2$, where $\Delta(B - R_\mathrm{c})$ is the offset in colour at fixed magnitude from the colour–magnitude relation of the red sequence. The red-sequence colour–magnitude zero-point was a median fit to all galaxies in a given cluster with $R_\mathrm{c} < 16$ mag, assuming a red-sequence slope of -0.06 mag mag^{-1}. These selection criteria were also applied to the model galaxies, ignoring the brighter limit of the zero-point fitting, which in practice makes little difference. One complication is that, for simplicity, B and R_c magnitudes were not computed directly in the models, but were instead determined from SDSS *gri* magnitudes using the transformations given in Blanton & Roweis (2007). Again, this makes little differ-

Table 1. Coma cluster observations.

Sample	N_gal	$\sigma^{200}_{\mathrm{H}\beta}$ (Å)	$\sigma^{200}_{\mathrm{Mg}\,b}$ (Å)	$\sigma^{200}_{\mathrm{Fe5270}}$ (Å)	$\sigma^{200}_{\mathrm{Fe5335}}$ (Å)
TFD08	12	0.032	0.033	0.037	0.041
Moore et al. (2002)	121	0.096	0.095	0.102	0.163
Nelan et al. (2005)	100	0.074	0.080	0.091	0.105

Note. Columns 3–6: mean index uncertainties for a galaxy with $\sigma = 200\,\mathrm{km\,s^{-1}}$.

© 2009 The Authors. Journal compilation © 2009 RAS, MNRAS **395,** 608–624

Downloaded from https://academic.oup.com/mnras/article-abstract/395/2/608/993417 by University of Groningen user on 13 December 2018

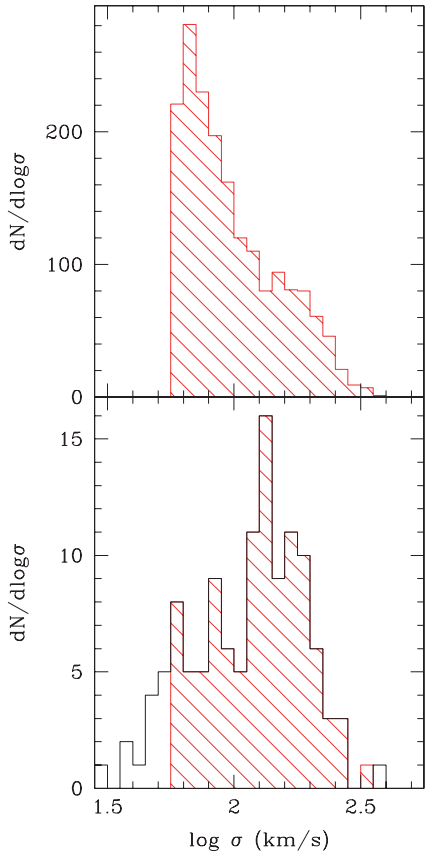

Figure 12. Top panel: VDF of model galaxies for a suite of 20 Coma-cluster-sized haloes. Bottom panel: VDF of observed Coma cluster galaxies in the Moore et al. (2002) sample (black) and of the mock catalogue built to match the Moore et al. (2002) galaxies (red hashed). Note that the VDF of the full suite is missing galaxies at the extrema of the observed VDF, and so these are also missing from the mock catalogue (see text).

ence in practice. Note that these red-sequence galaxies can have any morphology and are not selected to be early-type galaxies.

For each galaxy selected from the simulation to populate the VDF, the average errors in the line-strength indices of the observed galaxies *in that bin* are applied to the indices of that galaxy to determine its 'observed' indices and are labelled as its line-strength index errors. SSP-equivalent stellar population parameters are then determined from the 'observed' indices as described in Section 2.8.

4.4 Mock catalogues: comparison with observations

We begin by comparing the predictions of the models with the TFD08 LRIS sample. The predicted and observed line strengths are shown in Fig. 13. We see that the Hβ strengths of the observed and model galaxies are quite similar, but the [MgFe] strengths are too low. Fig. 14 shows that this discrepancy is driven by the metallicity offset mentioned above – the metallicities of the model galaxies are too low by ∼0.4 dex and have a too steep velocity-dispersion–metallicity relation (right-hand panels). The difference in metallicities is *not* entirely due to aperture effects, as we have shown in the Appendix that such effects can only change the metallicity by ∼0.1 dex. The left-hand panels of Fig. 14 show, however, that the observed and model (SSP-equivalent) ages are similar, although the models show a weak 'archaeological downsizing' effect that is not clearly present in the observations. Note that TFD08 claim that

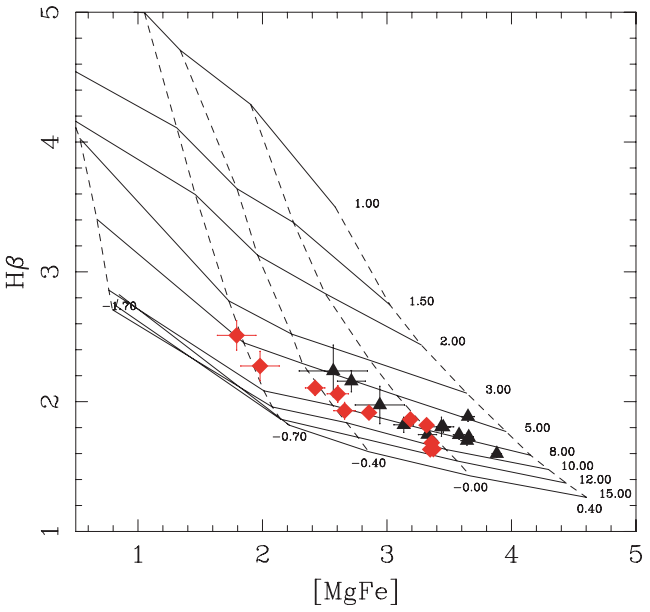

Figure 13. Observed (black) and mock (red) line strengths of the TFD08 sample. Model grids are the same as in Fig. 2. Note that the mock galaxies have a similar mean age (Hβ) as the bulk of observed sample – although the observed scatter is larger – but the metallicities ([MgFe]) are shifted too low.

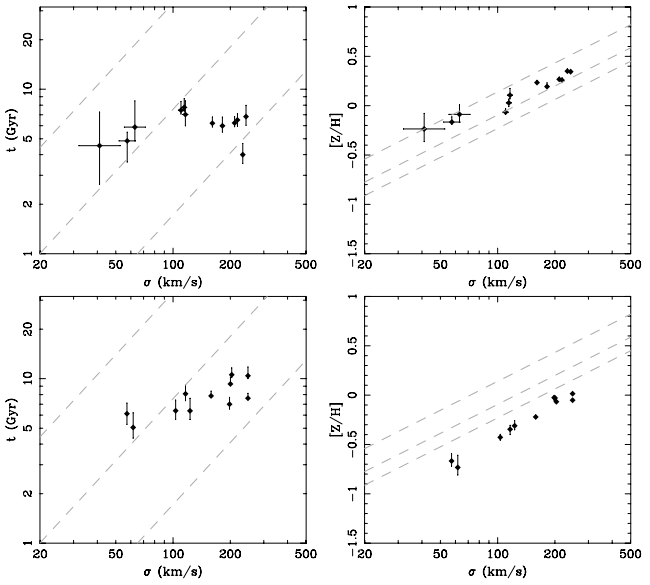

Figure 14. Velocity-dispersion–stellar-population relations for the observed (top panels) and mock (bottom panels) TFD08 sample (see Fig. 3). As in Fig. 13, the age distribution of the mock galaxies is similar to the observed galaxies (left-hand panels), although a bit steeper as a function of velocity dispersion, while the metallicities of the mock galaxies are too low (right-hand panels). This difference in metallicity is *not* entirely due to aperture effects, which can contribute only ∼0.1 dex of the difference (see text and the Appendix). The dashed lines are the projections of the observed Coma cluster Z plane (see Figs 3 and 10).

there is *no* 'archaeological downsizing' in this sample, but this is admittedly a very small sample. Examining the Z plane in Fig. 15, we find that, apart from the obvious metallicity offset, the current galaxy formation models produce a similar Z plane to that observed.

Downloaded from https://academic.oup.com/mnras/article-abstract/395/2/608/993417 by University of Groningen user on 13 December 2018

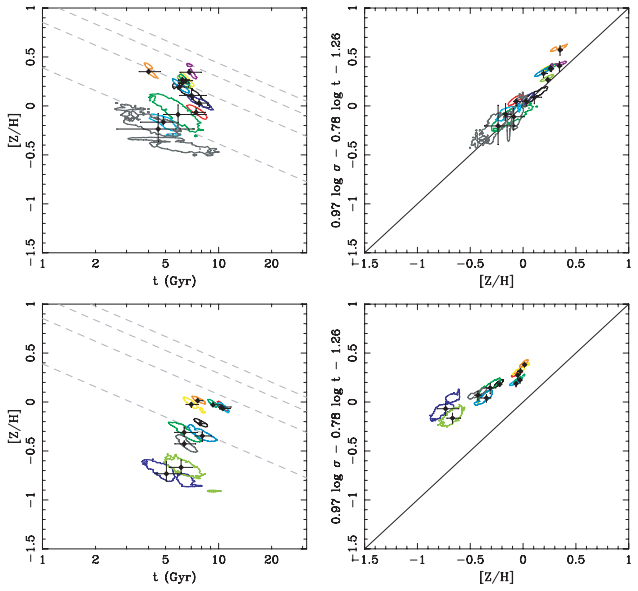

Figure 15. The nearly face-on (left-hand panels) and edge-on (right-hand panels) views of the Z plane (Trager et al. 2000b) in the observed (top panels) and mock (bottom panels) TFD08 sample. Contours are 68 per cent confidence intervals; note that the age–metallicity correlations are accentuated by but do not arise from the age–metallicity degeneracy. As in Figs 13 and 14, it is clear that the metallicity of the mock catalogue is too low, but the age distribution is similar. Again, the difference in metallicity is not entirely due to aperture effects (see text). The dashed lines are the projections of the observed Coma cluster Z plane (see Figs 3 and 10).

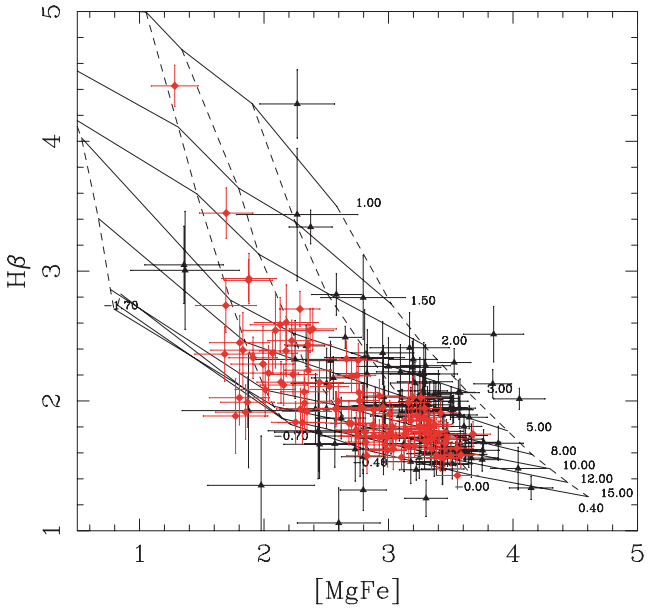

Figure 16. As for Fig. 13, but for the Moore et al. (2002) sample.

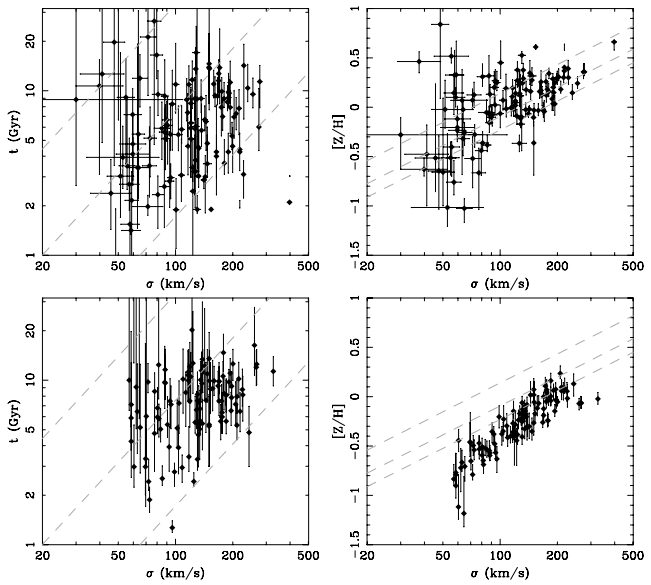

Figure 17. As for Fig. 14, but for the Moore et al. (2002) sample.

However, the slight correlation between $t_{\rm SSP}$ and $[Z/{\rm H}]_{\rm SSP}$ in the models seen in the bottom-left panel of this figure may be the cause of the too steep velocity-dispersion–metallicity relation seen in Fig. 14. Again, the LRIS sample is very small, but the quality of the data suggests that a large survey of a cluster like Coma with very high-quality data would be very instructive to probe these models even further (we pursue this idea below).

We repeat this exercise with the Moore and Nelan samples in Figs 16–21. It is clear from these figures that the poorer data quality of the Moore and Nelan samples makes definitive conclusions difficult, but the same trends seen in the LRIS sample are generally present. Although the lowest velocity dispersion model galaxies are missing due to the simulation mass limit (see above), there seems to be a lack of model galaxies with ages $t_{\rm SSP} < 4$ Gyr compared with the Moore et al. (2002) sample at $\sigma \lesssim 200\,{\rm km\,s^{-1}}$ in the left-hand panels of Fig. 17; the effect is less severe for the Nelan et al. (2005) sample (left-hand panels of Fig. 20). However, the errors in the observations are large enough to make a quantification of this result problematic.

It is also clear from the right-hand panels of Figs 17 and 20 that the mass–metallicity relations of the mock catalogues are steeper than those of the real data, as the large number of galaxies makes comparison of the relations easier than in Fig. 14, although this result is also apparent there. We again see an offset in the metallicities in these figures larger than the likely aperture effect. Using galaxy formation models with more detailed chemical evolution prescriptions by Arrigoni et al. (in preparation), we have found that the slope difference in the mass–metallicity relation is mostly corrected by the proper inclusion of SNe Ia in the chemical evolution model and that the metallicity offset can be corrected by a slight flattening of the IMF. However, proper inclusion of this more detailed modelling here is beyond the scope of this paper. The apparent smaller scatter in the metallicity distributions of the simulated galaxies at low velocity dispersion in the lower-right panels of Figs 17 and 20 is interesting, as the scatter in the data appears larger. It is likely that much of this scatter in the data is from observational uncertainties (e.g. poor emission-line correction and low S/N), but that may not explain all of the scatter, and the tightness of the model metallicities may be another problem in the current models. It would be interesting to attempt to reproduce the recent results of Smith et al. (2009), who studied dwarf galaxies at high S/N in the Coma cluster, to pursue this further.

We conclude from the comparison of these three surveys of Coma galaxies with their mock catalogues that the current semi-analytic models reproduce the present-day SSP-equivalent ages moderately well, although the agreement is not perfect. The model apparently does not have the correct SFHs for these objects, such that the 'archaeological downsizing' seen in model galaxies is stronger than

Downloaded from https://academic.oup.com/mnras/article-abstract/395/2/608/993417 by University of Groningen user on 13 December 2018

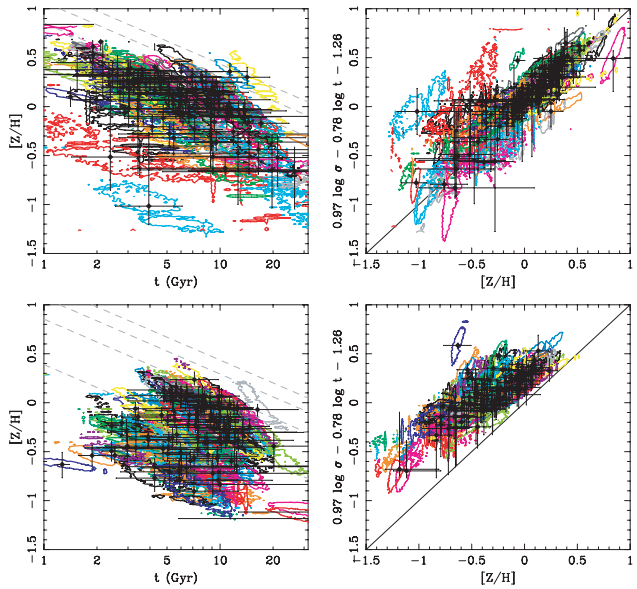

Figure 18. As for Fig. 15, but for the Moore et al. (2002) sample.

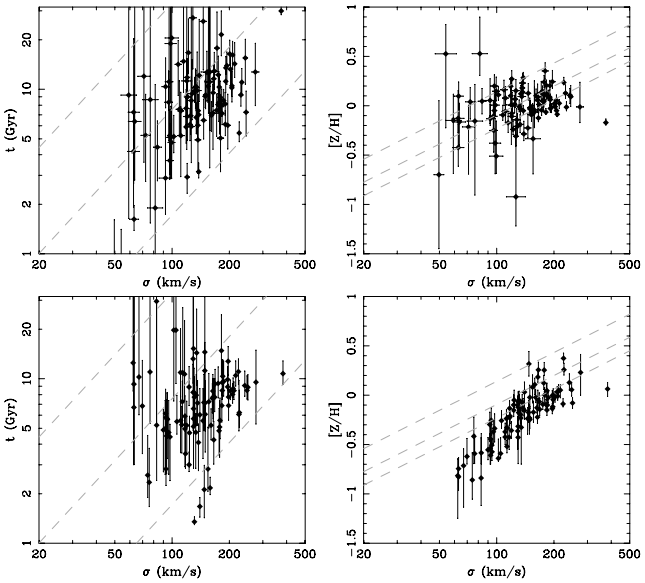

Figure 20. As for Fig. 14, but for the Nelan et al. (2005) sample.

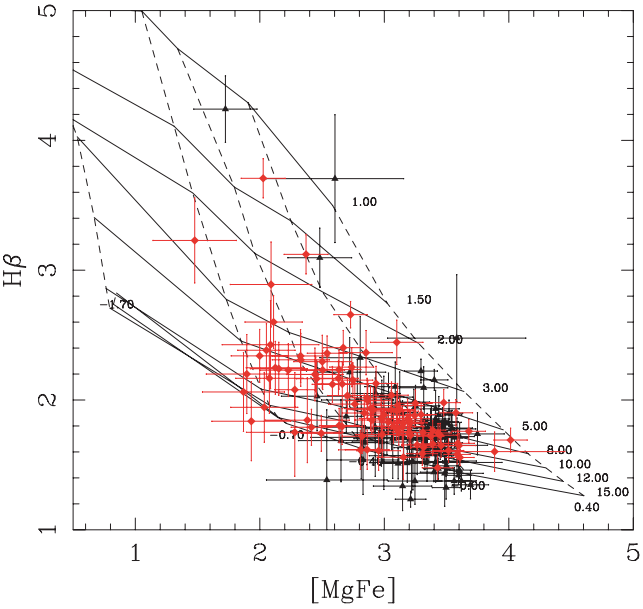

Figure 19. As for Fig. 13, but for the Nelan et al. (2005) sample.

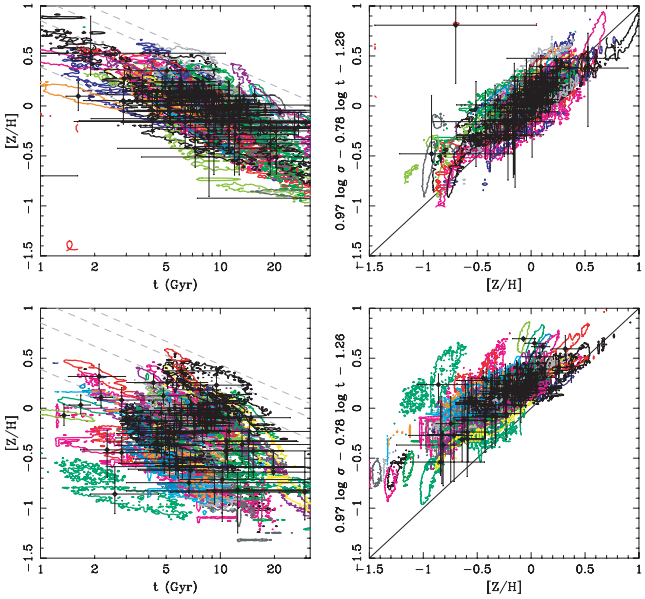

Figure 21. As for Fig. 15, but for the Nelan et al. (2005) sample.

in the best observations. However, the moderately good agreement between the SSP-equivalent ages of the mock catalogues and the data suggests that the star formation quenching recipe implemented in the hierarchical galaxy formation model produces roughly the correct amount of RSF and is therefore a reasonable if imperfect representation of the process suppressing star formation in these galaxies. The model metallicities are clearly problematic in large part due to known deficiencies with the simple chemical evolution prescription used here. We expect to correct these deficiencies in upcoming models (Arrigoni et al., in preparation).

4.5 Idealized nearby rich cluster surveys

In the previous section, we found that the currently available samples of Coma cluster galaxies are either too small or of too low quality to provide sharp tests of the hierarchical galaxy formation models. We now ask what could be learned from a spectroscopic survey of a Coma-sized cluster with roughly 100 galaxies (similar to the Moore et al. 2002 and Nelan et al. 2005 samples) with the data quality of the LRIS (TFD08) sample.

We create two different idealized large surveys: one selected solely by morphology to be early-type galaxies with any colour and one solely by colour to lie on the red sequence with any morphology (although both are mass-limited by the simulation itself). To be precise, we selected for the first sample early-type galaxies from the simulations to have the VDF of the Moore et al. (2002) sample and for the second the red-sequence colour–magnitude selection function and VDF of Smith et al. (2004). In both cases, we applied the line-strength uncertainties of the galaxy in the LRIS sample with

Downloaded from https://academic.oup.com/mnras/article-abstract/395/2/608/993417 by University of Groningen user on 13 December 2018

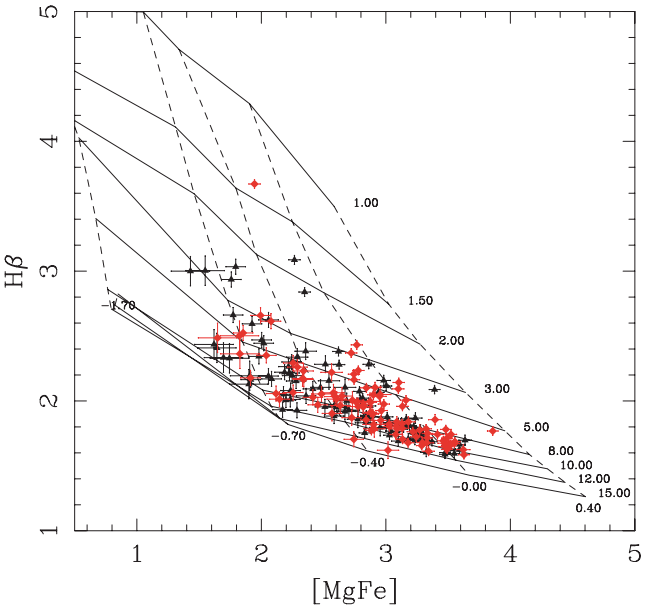

Figure 22. The absorption-line strengths of two idealized nearby rich cluster galaxy surveys. Black points are model galaxies selected to have early-type morphology; red points are model galaxies selected to be on the red sequence (with the same limits as the Nelan et al. 2005 sample). Model grids as in Fig. 2. Both mock catalogues have the same line-strength errors as the TFD08 sample; the morphology-selected sample has the same number of galaxies and VDF as the Moore et al. (2002, see Fig. 12, bottom panel) sample and the red-sequence-colour-selected sample has the same number of galaxies and VDF as the Nelan et al. (2005) sample. The age, metallicity and enhancement ratio distributions of these samples can be easily determined with such a large sample with such small uncertainties. Nearly all young, metal-rich galaxies in the red-sequence sample are dusty late-type galaxies.

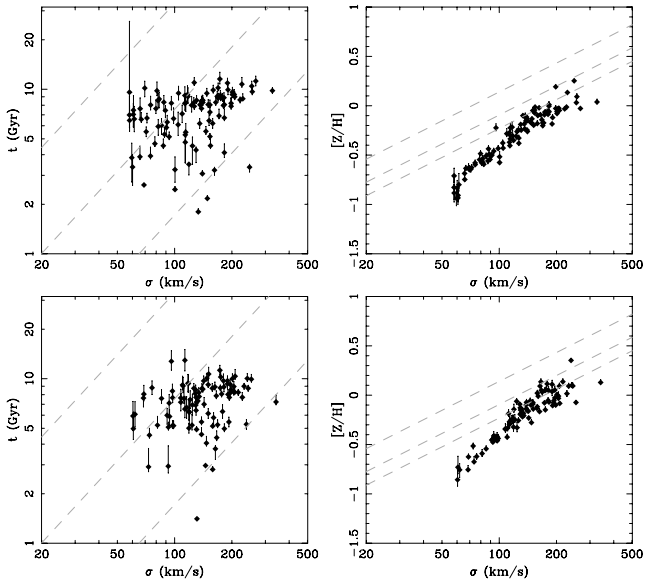

Figure 23. The predicted velocity dispersion-stellar population relations for two idealized nearby rich cluster surveys. Top panel: morphology-selected sample. Points with large error bars in age (right-hand panel) are those that sit very close to or off the bottom of the SSP model grids in Fig. 22. Bottom panel: red-sequence-colour-selected sample. As in Fig. 22, the age, metallicity and enhancement ratio distributions can be easily measured from such surveys, but the 'archaeological downsizing' seen in mass-weighted age in Fig. 4 is difficult to see even in this sample.

velocity dispersion nearest to each model galaxy to the model line strengths.

We plot the resulting line strengths in Fig. 22 and SSP-equivalent parameters as functions of velocity dispersion in Fig. 23. Note that the early-type galaxy sample has more young ($t_{\rm SSP} < 5$) galaxies than the red-sequence sample; these are blue early-type galaxies, absent from the latter sample. Nearly all of the young, metal-rich galaxies in the red-sequence sample are dusty, late-type (spiral) galaxies in the simulation. On the other hand, it appears that there may be more low-mass, old but metal-poor galaxies in the early-type galaxy sample than in the red-sequence sample. This is apparently a result of the magnitude limit of the latter sample, which selects against the smallest and therefore metal-poorest galaxies; however, this is a small effect, as the magnitude limit of the red-sequence selection ($R_{\rm c} < 17$) is close to the mass limit in our simulation for old galaxies at this redshift (Fig. 11).

It is clear from Figs 22–24 that a large, high-quality survey of a Coma-sized cluster would provide a wealth of information on the precise distribution of stellar population parameters in early-type and/or red-sequence cluster galaxies, showing any deviations from or curvature of the Z plane and providing stringent tests of both hierarchical galaxy formation models and previous data. As a simple but interesting example, such a survey would answer the question posed by TFD08 (see also Sánchez-Blázquez et al. 2006a,b): are the nearly constant ages of early-type Coma cluster galaxies just a selection effect resulting from observing only 12 galaxies or is this a general result for the entire cluster?

5 CONCLUSIONS

In this study we set out to use hierarchical galaxy formation models to understand the properties of local galaxies and, conversely, to use those properties to test hierarchical galaxy formation models. To accomplish these goals, we make use of a state-of-the-art semi-analytic galaxy formation model that includes a well-calibrated parametrization of galaxy mergers, BH growth and both 'bright' and 'radio mode' feedback from these BHs. We coupled these cosmologically motivated models to stellar population models to produce synthetic spectra and computed line strengths from these spectra. We then used the line strengths to determine 'SSP-equivalent' ages and compositions *in precisely the same way as for the observed spectra*.

We created 20 realizations of a simulated Coma-cluster-sized halo for this study in order to compare our results with recent studies of early-type galaxies in the Coma cluster (Moore et al. 2002; Nelan et al. 2005; TFD08). We began by comparing the inferred SSP-equivalent ages and compositions of *model* early-type galaxies with the mass- and light-weighted ages and compositions of these model galaxies. We found that SSP-equivalent ages are (at best) biased tracers of mass- or light-weighted ages, and are always younger than these 'true' ages. This is because hot, young stars contribute much more strongly per unit mass to the Balmer lines than old stars (Trager et al. 2000b, 2005; Serra & Trager 2007). The bias of SSP-equivalent ages towards young ages implies that the 'archaeological' or 'fossil downsizing' seen in previous studies (e.g. Nelan et al. 2005; Thomas et al. 2005; Clemens et al. 2006) overstates the 'true' downsizing in the early-type galaxy population. Rather, we find that the SSP-equivalent age correlates most strongly with the fraction of stars formed within the past Gyr. On the other hand, the SSP-equivalent metallicity is an excellent tracer of the light-weighted metallicity and a very good tracer of the mass-weighted metallicity

Downloaded from https://academic.oup.com/mnras/article-abstract/395/2/608/993417 by University of Groningen user on 13 December 2018

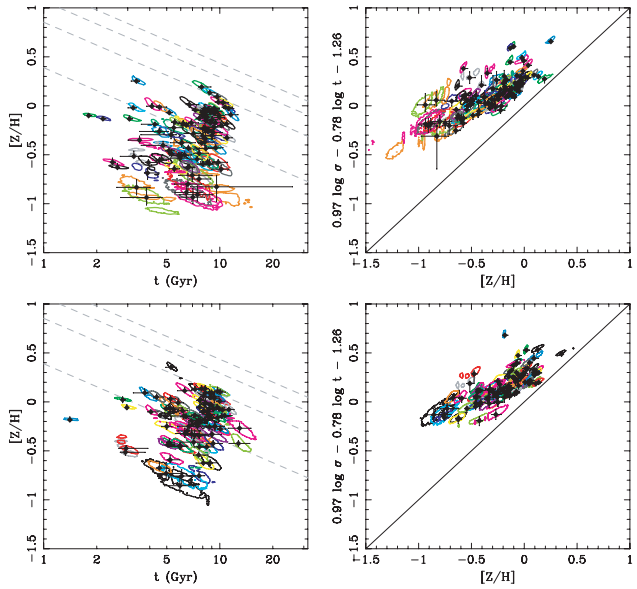

Figure 24. As in Figs 15 and 18, for two idealized nearby rich cluster surveys. Top panel: morphology-selected sample. Bottom panel: red-sequence-colour-selected sample. In comparison with Fig. 18, the error contours are small enough to see clear deviations from the plane, as well as any curvature that may be present.

of a galaxy. This is because hot, young stars contribute little to the metal lines in a composite spectrum (Trager et al. 2005; Serra & Trager 2007). These conclusions strengthen previous suggestions about the behaviour of line-strength-derived ages and metallicities based on simple two-burst stellar population models but extend them to more complex and, presumably, more realistic SFHs from a fully cosmological hierarchical galaxy formation model.

We then extracted mock catalogues from the simulation to represent three recent line-strength surveys of early-type galaxies in the Coma cluster: Moore et al. (2002), Nelan et al. (2005) and TFD08. These mock catalogues were intended to help us both to interpret the observations and to test the galaxy formation model itself. Unfortunately, drawing significant conclusions about the SFHs of Coma cluster galaxies was not possible: the size of the high-quality sample (TFD08) was too small, while the data quality of the large samples (Moore et al. 2002; Nelan et al. 2005) was too poor. We could however note some interesting problems with the model from discrepancies between the mock catalogues and the observed samples. First, comparison of the observed velocity-dispersion–metallicity relations with the models revealed that the models are currently producing neither the correct zero-point of these relations – the model galaxies are too metal-poor – nor the correct slope. The former problem is likely to be due to the lack of SNe Ia nucleosynthesis in the current models, while the latter problem has two likely causes: (1) the SFHs of the model galaxies are not the same as real galaxies, such that the variation of $t_{\rm SSP}$ with velocity dispersion is too steep in the models compared with the data (left-hand panels of Fig. 14), leading to an incorrect $t_{\rm SSP} - [Z/{\rm H}]_{\rm SSP}$ relation (left-hand panels of Fig. 15) and (2) the assumed IMF may not be correct (Arrigoni et al., in preparation). That being said, the reasonable agreement between the SSP-equivalent ages of the mock catalogues and the observed samples suggests that, while imperfect, the star formation quenching model implemented in the hierarchical galaxy formation models is a reasonable representation of the true process suppressing star formation in early-type galaxies. We suggest that a large, deep, high-quality survey of a cluster like Coma – easily achievable with the current generation of wide-field spectrographs on 8–10-m class telescopes – would provide a sharp test for the models that is not yet possible with the current data sets.

We have shown that the combination of hierarchical galaxy formation models with detailed stellar population models provides powerful tools both for understanding the stellar populations of early-type galaxies and for testing the hierarchical galaxy formation models themselves. We look forward to better data sets and to more realistic models for both galaxy formation and stellar populations. As has been mentioned several times, we are currently working on one of these aspects, introducing a detailed treatment of multi-element chemical evolution into the semi-analytic galaxy formation models (Arrigoni et al., in preparation). These enhanced models will allow us to probe the SFHs of galaxies – and test the galaxy formation models – much more robustly and thoroughly than previously possible.

ACKNOWLEDGMENTS

We would like to thank Sandy Faber for suggesting the combination of semi-analytic and stellar population models that inspired this study. Peter Polko developed an early version of these models, for which we are grateful. We also thank Matías Arrigoni for a careful reading of the manuscript, Eric Bell, Richard Bower and Paolo Serra for stimulating conversations and the anonymous referee for suggestions that helped us to clarify the presentation. Finally, we thank the directors of the Max-Planck-Institut für Astronomie, Hans-Walter Rix, and the Kapteyn Astronomical Institute, J.M. van der Hulst, and the Leids Kerkhoven-Bosscha Fonds for providing travel support and working space during the gestation of this paper.

REFERENCES

Adelman-McCarthy J. K. et al., 2008, ApJS, 175, 297
Baldry I. K., Glazebrook K., Brinkmann J., Ivezić Ž., Lupton R. H., Nichol R. C., Szalay A. S., 2004, ApJ, 600, 681
Bernardi M., Sheth R. K., Nichol R. C., Schneider D. P., Brinkmann J., 2005, AJ, 129, 61
Bernardi M., Nichol R. C., Sheth R. K., Miller C. J., Brinkmann J., 2006, AJ, 131, 1288
Bertelli G., Bressan A., Chiosi C., Fagotto F., Nasi E., 1994, A&AS, 106, 275
Blanton M. R., Roweis S., 2007, AJ, 133, 734
Blumenthal G. R., Faber S. M., Primack J. R., Rees M. J., 1984, Nat, 311, 517
Bower R. G., Benson A. J., Malbon R., Helly J. C., Frenk C. S., Baugh C. M., Cole S., Lacey C. G., 2006, MNRAS, 370, 645
Bruzual G., Charlot S., 2003, MNRAS, 344, 1000 (BC03)
Buzzoni A., Mantegazza L., Gariboldi G., 1994, AJ, 107, 513
Cardelli J., Clayton G., Mathis J., 1989, ApJ, 345, 245
Cardiel N., Gorgas J., Cenarro J., Gonzalez J. J., 1998, A&AS, 127, 597
Cardiel N., Gorgas J., Sánchez-Blázquez P., Cenarro A. J., Pedraz S., Bruzual G., Klement J., 2003, A&A, 409, 511
Cattaneo A., Dekel A., Devriendt J., Guiderdoni B., Blaizot J., 2006, MNRAS, 370, 1651
Chabrier G., 2001, ApJ, 554, 1274
Charlot S., Fall S. M., 2000, ApJ, 539, 718
Clemens M. S., Bressan A., Nikolic B., Alexander P., Annibali F., Rampazzo R., 2006, MNRAS, 370, 702
Cole S., Aragon-Salamanca A., Frenk C. S., Navarro J. F., Zepf S. E., 1994, MNRAS, 271, 781
Cox T. J., Jonsson P., Somerville R. S., Primack J. R., Dekel A., 2008, MNRAS, 384, 386

Downloaded from https://academic.oup.com/mnras/article-abstract/395/2/608/993417 by University of Groningen user on 13 December 2018

Croton D. J. et al., 2006, MNRAS, 365, 11
Davies R. L., Sadler E. M., Peletier R. F., 1993, MNRAS, 262, 650
De Lucia G., Blaizot J., 2007, MNRAS, 375, 2
De Lucia G., Springel V., White S. D. M., Croton D., Kauffmann G., 2006, MNRAS, 366, 499
Di Matteo T., Springel V., Hernquist L., 2005, Nat, 433, 604
Faber S. M., 1973, ApJ, 179, 731
Gallazzi A., Charlot S., Brinchmann J., White S. D. M., Tremonti C. A., 2005, MNRAS, 362, 41
González J. J., 1993, PhD thesis, Univ. California
Graves G. J., Faber S. M., Schiavon R. P., Yan R., 2007, ApJ, 671, 243
Häring N., Rix H.-W., 2004, ApJL, 604, L89
Heavens A. F., Jimenez R., Lahav O., 2000, MNRAS, 317, 965
Hopkins P. F., Hernquist L., Cox T. J., Robertson B., Krause E., 2007, ApJ, 669, 45
Hudson M. J., Lucey J. R., Smith R. J., Schlegel D. J., Davies R. L., 2001, MNRAS, 327, 265
Jimenez R., Bernardi M., Haiman Z., Panter B., Heavens A. F., 2007, ApJ, 669, 947
Kauffmann G., 1996, MNRAS, 281, 487
Kauffmann G., Charlot S., 1998, MNRAS, 294, 705
Kauffmann G., White S. D. M., Guiderdoni B., 1993, MNRAS, 264, 201
Kennicutt R., 1989, ApJ, 344, 685
Kennicutt R., 1998, ApJ, 498, 181
Kubo J. M., Stebbins A., Annis J., Dell'Antonio I. P., Lin H., Khiabanian H., Frieman J. A., 2007, ApJ, 671, 1466
Kuntschner H., 2000, MNRAS, 315, 184
Kuntschner H., Lucey J. R., Smith R. J., Hudson M. J., Davies R. L., 2001, MNRAS, 323, 615
Lintott C. J., Ferreras I., Lahav O., 2006, ApJ, 648, 826
Łokas E. L., Mamon G. A., 2003, MNRAS, 343, 401
MacArthur L. A., 2005, ApJ, 623, 795
Mehlert D., Saglia R. P., Bender R., Wegner G., 2000, A&AS, 141, 449
Moore S. A. W., Lucey J. R., Kuntschner H., Colless M., 2002, MNRAS, 336, 382
Nelan J. E., Smith R. J., Hudson M. J., Wegner G. A., Lucey J. R., Moore S. A. W., Quinney S. J., Suntzeff N. B., 2005, ApJ, 632, 137
Nulsen P. E. J., Fabian A. C., 2000, MNRAS, 311, 346
O'Connell R. W., 1986, in Norman C. A., Renzini A., Tosi M., eds, Stellar Populations. Cambridge Univ. Press, Cambridge, p. 167
Ocvirk P., Pichon C., Lançon A., Thiébaut E., 2006, MNRAS, 365, 46
Oke J. B. et al., 1995, PASP, 107, 375
Panter B., Heavens A. F., Jimenez R., 2003, MNRAS, 343, 1145
Rabin D., 1982, ApJ, 261, 85
Reichardt C., Jimenez R., Heavens A. F., 2001, MNRAS, 327, 849
Renzini A., 2006, ARA&A, 44, 141
Robertson B., Cox T. J., Hernquist L., Franx M., Hopkins P. F., Martini P., Springel V., 2006, ApJ, 641, 21
Sánchez-Blázquez P., Gorgas J., Cardiel N., González J. J., 2006a, A&A, 457, 787
Sánchez-Blázquez P., Gorgas J., Cardiel N., González J. J., 2006b, A&A, 457, 809
Schiavon R. P., 2007, ApJS, 171, 146
Serra P., Trager S. C., 2007, MNRAS, 374, 769
Simien F., de Vaucouleurs G., 1986, ApJ, 302, 564
Smith R. J. et al., 2004, AJ, 128, 1558
Smith R. J., Lucey J. R., Hudson M. J., Allanson S. P., Bridges T. J., Hornschemeier A. E., Marzke R. O., Miller N. A., 2009, MNRAS, 392, 1265
Somerville R. S., Kolatt T. S., 1999, MNRAS, 305, 1
Somerville R. S., Primack J. R., 1999, MNRAS, 310, 1087
Somerville R. S., Primack J. R., Faber S. M., 2001, MNRAS, 320, 504
Somerville R. S. et al., 2004, ApJL, 600, L135
Somerville R. S. et al., 2008a, ApJ, 672, 776
Somerville R. S., Hopkins P. F., Cox T. J., Robertson B., Hernquist L., 2008b, MNRAS, 391, 481 (S08)
Spergel D. N. et al., 2007, ApJS, 170, 377
Springel V., White S. D. M., Tormen G., Kauffmann G., 2001, MNRAS, 328, 726
Springel V., Di Matteo T., Hernquist L., 2005, MNRAS, 361, 776
Strateva I. et al., 2001, AJ, 122, 1861
Thomas D., Maraston C., Bender R., 2003, MNRAS, 339, 897
Thomas D., Maraston C., Korn A., 2004, MNRAS, 351, L19
Thomas D., Maraston C., Bender R., Mendes de Oliveira C., 2005, ApJ, 621, 673
Thomas D., Maraston C., Schawinski K., Sarzi M., Joo S.-J., Kaviraj S., Yi S. K., 2007, in Vazdekis A., Peletier R. F., eds, Proc. IAU Symp. 241, Stellar Populations as Building Blocks of Galaxies. Cambridge Univ. Press, Cambridge, p. 546
Tojeiro R., Heavens A. F., Jimenez R., Panter B., 2007, MNRAS, 381, 1252
Toomre A., 1977, in Tinsley B. M., Larson R. B., eds, Evolution of Galaxies and Stellar Populations. Yale Univ. Press, New Haven, p. 401
Trager S. C., 1997, PhD thesis, Univ. California
Trager S. C., Faber S. M., Worthey G., González J. J., 2000a, AJ, 119, 1645
Trager S. C., Faber S. M., Worthey G., González J. J., 2000b, AJ, 120, 165
Trager S. C., Worthey G., Faber S. M., Dressler A., 2005, MNRAS, 362, 2
Trager S. C., Faber S. M., Dressler A., 2008, MNRAS, 386, 715 (TFD08)
Vazdekis A., Casuso E., Peletier R. F., Beckman J. E., 1996, ApJS, 106, 307
White S. D. M., Rees M. J., 1978, MNRAS, 183, 341
Worthey G., 1994, ApJS, 95, 107
Worthey G., Ottaviani D. L., 1997, ApJS, 111, 377

APPENDIX A: APERTURE CORRECTIONS

Unfortunately, the Coma cluster is not quite far enough away for its member galaxies to be completely contained in a reasonably sized slit or fibre. A fair comparison of the observational data with the galaxy formation models requires corrections to be made for the fact that early-type galaxies have line-strength gradients (see, e.g., Davies, Sadler & Peletier 1993; González 1993; Mehlert et al. 2000, among many others). We must therefore estimate the effect of these gradients on the stellar population parameters.

To make the required corrections, we appeal to the high-quality line-strength gradient measurements of González (1993). González measured gradients in 40 local early-type galaxies, typically along both the major and minor axes. We have used his 'elliptical-aperture-weighted' line strengths (see his Chapter 5) and taken error-weighted averages, where possible, of the major and minor axis line strengths in apertures of radii $r = r_e/16$, $r_e/8$, $r_e/4$ and $r_e/2$ (if only one axis was available, we used that axis). We then fit linear relations of the form

$$\log I(r/r_e) = a + b \log(r/r_e), \tag{A1}$$

where $I(r/r_e)$ is the line strength within an elliptical aperture with the fractional equivalent circular radius r/r_e. We define $b = \mathrm{d}\log I(r/r_e)/\mathrm{d}\log(r/r_e)$, the line-strength gradient for each galaxy. To search for trends in these gradients as a function of, e.g., velocity dispersion, we plot the results as a function of $\log\sigma(r = r_e/4)$ in Fig. A1. We find only minimal hints of trends with velocity dispersion and a very large scatter, so we use the error-weighted mean of the gradients from *all* galaxies for each index to estimate our aperture corrections. These means are tabulated in Table A1. The final (logarithmic) line strengths at one effective radius – a reasonable guess at a 'global' value – are then taken to be

$$\log I(r_e) = \log I(r) + \langle b \rangle * \log(r/r_e), \tag{A2}$$

where $\langle b \rangle$ is the mean gradient of index I and r is the radius of the original aperture: for the LRIS data, $r = r_e/4$; for the Moore

Downloaded from https://academic.oup.com/mnras/article-abstract/395/2/608/993417 by University of Groningen user on 13 December 2018

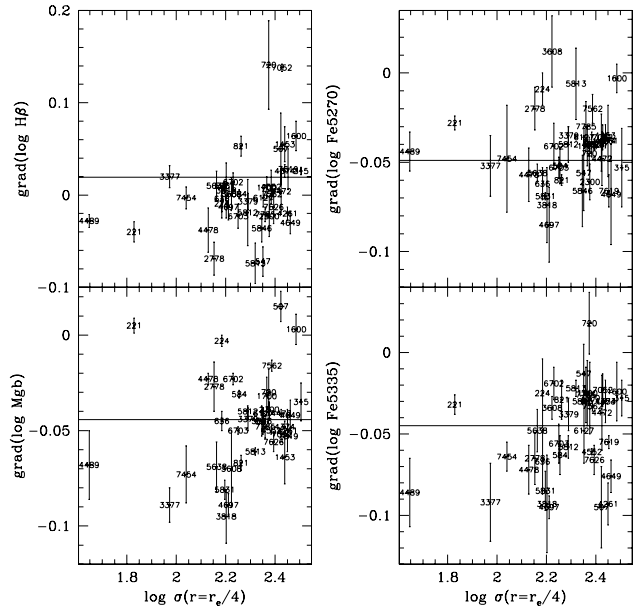

Figure A1. Line-strength gradients in elliptical apertures derived from González (1993), in the sense d log I/d log (r/r_e) (see text for more details). Solid lines are error-weighted means of the index gradients.

Table A1. Mean line-strength gradients derived from González (1993).

Index	d log I/d log (r/r_e)
Hβ	0.019 ± 0.051
Mg b	-0.044 ± 0.018
Fe5270	-0.049 ± 0.018
Fe5335	-0.045 ± 0.022

sample, $r = 1.35$ arcsec, and for the Nelan sample, $r = 1.0$ arcsec. The errors in the mean gradients are added in quadrature (after scaling by the logarithmic difference in the radii) to the original line-strength errors.

Table A2. Stellar population gradients.

Parameter	$r_e/4 \rightarrow r_e$	$1\farcs35 \rightarrow r_e$
log t	0.01 ± 0.05	0.01 ± 0.05
[Z/H]	-0.10 ± 0.03	-0.10 ± 0.03
[E/Fe]	0.00 ± 0.01	0.00 ± 0.01

We estimate the mean shifts incurred in the stellar population parameters when scaling from the LRIS and Moore apertures to 'global' $r = r_e$ apertures. Unfortunately, we do not have measured effective radii for many of the galaxies in the Moore sample. We have however measured the line strengths and stellar population parameters of the LRIS galaxies in an equivalently sized aperture as Moore et al. (2002). The results are presented in Table A2. As expected (see, e.g., Trager et al. 2000b), we find a slight difference in the metallicity, such that the galaxies are 0.10 ± 0.03 dex more metal-poor in the 'global' r_e aperture than in the smaller apertures. We find, however, negligible differences (less than 3 per cent in each parameter) between the ages and enhancement ratios in the larger and smaller apertures.

This paper has been typeset from a TEX/LATEX file prepared by the author.

Downloaded from https://academic.oup.com/mnras/article-abstract/395/2/608/993417 by University of Groningen user on 13 December 2018